Journal of Molecular Spectroscopy 393 (2023) 111778

Contents lists available at ScienceDirect

Journal of Molecular Spectroscopy

journal homepage: www.elsevier.com/locate/yjmsp

Spectroscopic study of the $F^1\Sigma_g^+$ outer well state in H_2, HD and D_2

K.-F. Lai, M. Beyer, W. Ubachs *

Department of Physics and Astronomy, LaserLaB, Vrije Universiteit, De Boelelaan 1081, 1081 HV Amsterdam, The Netherlands

ARTICLE INFO

Keywords:
Molecular hydrogen
Multi-photon ionization
Double-well potentials
UV-laser

ABSTRACT

Two-photon UV-photolysis of hydrogen sulfide molecules is applied to produce hydrogen molecules in highly excited vibrational levels in the $X^1\Sigma_g^+$ electronic ground state, up to the dissociation energy and into the quasibound region. Photolysis precursors H_2S, HDS and D_2S are used to produce vibrationally hot H_2, HD and D_2. The wave function density at large internuclear separation is excited via two-photon transitions in the $F^1\Sigma_g^+$ - $X^1\Sigma_g^+$ system to probe ro-vibrational levels in the first $F^1\Sigma_g^+$ outer well state of *gerade* symmetry. Combining with accurate knowledge of the $X^1\Sigma_g^+(v, J)$ levels from advanced ab initio calculations, energies of rovibrational levels in the $F^1\Sigma_g^+$ state are determined. For the H_2 isotopologue a three-laser scheme is employed yielding level energies at accuracies of 4×10^{-3} cm^{-1} for $F(v = 0, J)$ up to $J = 21$ and for some low J values of $F(v = 1)$. A two-laser scheme was applied to determine level energies in H_2 for $F(v = 0 - 4)$ levels as well as for various F levels in HD and D_2, also up to large rotational quantum numbers. The latter measurements in the two-laser scheme are performed at lower resolution and the accuracy is strongly limited to 0.5 cm^{-1} by ac-Stark effects. For H_2 a new quasibound resonance $X^1\Sigma_g^+(v = 6, J = 23)$ is detected through the Q(23) and O(23) transitions in the F0-X6 band. Also a quasi-bound resonance in D_2 is assigned, for the first time in this species: $X^1\Sigma_g^+(v = 17, J = 15)$. The experimental results on $F(v, J)$ level energies are compared with previously reported theoretical results from multi-channel quantum-defect calculations as well as with results from newly performed non-adiabatic quantum calculations.

1. Introduction

The potential energy level structure of the hydrogen molecule, the smallest neutral molecule, is of a peculiar nature. Strong couplings occur between singly- and double-excited electronic states, with also the ion-pair configuration interacting at large internuclear separation. The small mass of the hydrogen atom allows for strong adiabatic and nonadiabatic interactions between these electronic manifolds resulting in double-well structures for the potential energy curves of the hydrogen molecule.

Based on the early spectroscopic studies by Dieke [1,2] Davidson concluded that the first excited state of *gerade* symmetry is associated with a double-well potential energy curve [3]. Later this work was followed by more advanced quantum ab initio calculations of this lowest $EF^1\Sigma_g^+$ and higher-lying double-well potentials [4]. Precision laser spectroscopic studies focused mainly on rovibrational levels in the $E^1\Sigma_g^+$ inner well part [5–10].

The next higher double-well potential of *gerade* symmetry, denoted as $II'^1\Pi_g$, predicted by Mulliken [11] and later calculated by ab initio methods [4,12], exhibits a shallow outer well some 200 cm^{-1} below the $n = 2$ dissociation limit. Laser excitation to the large internuclear separation in the outer well was accomplished by multi-step excitation for both H_2 and D_2 [13] as well as for HD [14].

Higher-lying double-well states of *gerade* symmetry are the $GK^1\Sigma_g^+$ state [15,16] and the $H\bar{H}^1\Sigma_g^+$ state [17], which were both investigated via multi-step laser excitation. Besides this progression of double-well states in the *gerade* manifold of hydrogen there is also a double-well structure in the *ungerade* manifold, the $B''\bar{B}^1\Sigma_u^+$ state, which was excited in a three-laser excitation scheme [18,19]. Higher-lying double-well states in the *ungerade* manifold were predicted with outer wells at very large internuclear separation [20]. Attempts to observe rovibrational levels in these higher lying states had limited success [21].

Levels in the $F^1\Sigma_g^+$ outer well were investigated via emission studies with optical decay from higher lying electronic states exhibiting wave function density at 4–5 a_0. The initial studies by Dieke [1,2] were superseded by high-resolution Fourier-transform emission studies both for H_2 [22] and D_2 [23], but these were limited to rotational quantum numbers of $J \leq 5$. Direct two-photon laser excitation from the $X^1\Sigma_g^+(v = 0)$ ground state in H_2 was pursued to probe levels in the $F^1\Sigma_g^+$ outer well. Notwithstanding the small Franck–Condon factors this was successful although only levels with $v_F = 2, 3$ could be detected [24].

* Corresponding author.
E-mail address: w.m.g.ubachs@vu.nl (W. Ubachs).

https://doi.org/10.1016/j.jms.2023.111778
Received 14 February 2023; Received in revised form 10 April 2023; Accepted 10 April 2023
Available online 14 April 2023
0022-2852/© 2023 Vrije Universiteit Amsterdam. Published by Elsevier Inc. This is an open access article under the CC BY license (http://creativecommons.org/licenses/by/4.0/).

Steadman and Baer found an alternative route for the production of quantum states $H_2(v)$ at large internuclear separation, through the two-photon UV-photolysis of hydrogen sulfide (H_2S) [25]. Detailed studies following this idea were carried out in two- and three-laser schemes disentangling the steps of photodissociation and spectroscopy of the $F^1\Sigma_g^+X^1\Sigma_g^+$ system [26–28]. Use of a narrowband ultraviolet laser for the $F^1\Sigma_g^+X^1\Sigma_g^+$ spectroscopy step under Doppler-free conditions led to a test of QED in the highest bound levels $X^1\Sigma_g^+(v)$ in H_2, with $v = 13$ and 14 [29]. Ultimately, these studies were extended to the region above the $X^1\Sigma_g^+$ dissociation threshold with the detection and precision study of quasibound resonances in H_2 [30,31]. Quinn et al. explored another photolysis route, choosing formaldehyde (H_2CO) as a precursor to produce and study excitation from intermediate vibrational levels $X^1\Sigma_g^+(v = 3-9)$ in H_2, providing access to the $F^1\Sigma_g^+$ outer well for levels with $v_F = 4$, although in weak transitions [32].

In the present work the study of $F^1\Sigma_g^+$ - $X^1\Sigma_g^+$ two-photon transitions, involving hydrogen sulfide photolysis as a preparation step, was extended to the HD and D_2 isotopologues. For the first time a comprehensive study of $F^1\Sigma_g^+$ outer well levels in the mixed HD isotopologue was carried out. Quadrelli et al. [33] had performed an ab initio calculation including non-adiabatic couplings for $J = 0-5$ levels, which they had compared with early spectroscopic data for HD [1,34]. Combining the spectroscopic results for F - X two-photon transitions with accurately computed level energies of $X^1\Sigma_g^+(v, J)$ [35,36] leads to the determination of $F(v, J)$ level energies, here collected for all three isotopologues.

2. UV photolysis of hydrogen sulfide

The present study is an extension of previous studies on highly excited ro-vibrational quantum states in H_2 [29,31], now also probing highly excited states in HD and D_2. Such states are produced via two-photon UV-photolysis of hydrogen sulfide parent molecules. For two-photon photolysis at a UV-laser wavelength of 281.8 nm, the $3d\ ^1A_1$ electronic state is excited in all three isotopologues of the hydrogen sulfide parent molecule. This follows the assignment of Ashfold et al. [37], who had studied the 2 + 1 REMPI spectra of H_2S and D_2S in the range of 245–316 nm. The isotope shift of this electronic band is less than 100 cm^{-1} for D_2S and to be expected smaller for HDS. In Fig. 1 a 2 + 1 REMPI spectrum for both H_2S and D_2S molecules is shown, indicating the frequency positions of the two-photon photolysis resonances in the parent molecules. Since for the studies of HD a gas mixture of parent molecules with a large fraction of H_2S was used (see below) no clear and unambiguous REMPI spectra of HDS could be obtained.

In the F-X spectroscopy experiment the wavelength of the photolysis laser was chosen to maximize H_2^+, D_2^+ or HD^+ ion signals from the targeted hydrogen sulfide isotopologues. In the first stage of the current project the $4p\ ^1A_1$ resonance in the parent molecule was used (at λ_{UV} = 292 nm) for the photolysis step, providing access to the fragment states $H_2(v'' = 11, 12)$ [26–28]. The main body of the work employed λ_{UV} = 281.8 nm [29,31]. Also photolysis pathways were explored through the higher lying $4d\ ^1A_1$ electronic state with $\lambda_{UV} = 259.9$ nm, as well as the $4f\ ^1A_1$ state with $\lambda_{UV} = 257.9$ nm.

Following explorative studies by Steadman and Baer [25], ultraviolet laser photolysis of hydrogen sulfide is applied to produce molecular hydrogen in its ground $X^1\Sigma_g^+$ electronic state via the pathway:

$$XYS \xrightarrow{2h\nu} S(^1D_2) + XY,$$

with X, Y being H or D. The two-photon energy provided for the photolysis, amounting about 70 980 cm^{-1} (for λ_{UV} = 281.8 nm), is sufficient to overcome the dissociation energy of individual hydrogen sulfide isotopologues [29,31]. The dissociation energy (D_0) of H_2S in the $S(^1D_2)$ limit has been experimentally determined to be 69 935(25) cm^{-1} [38,39].

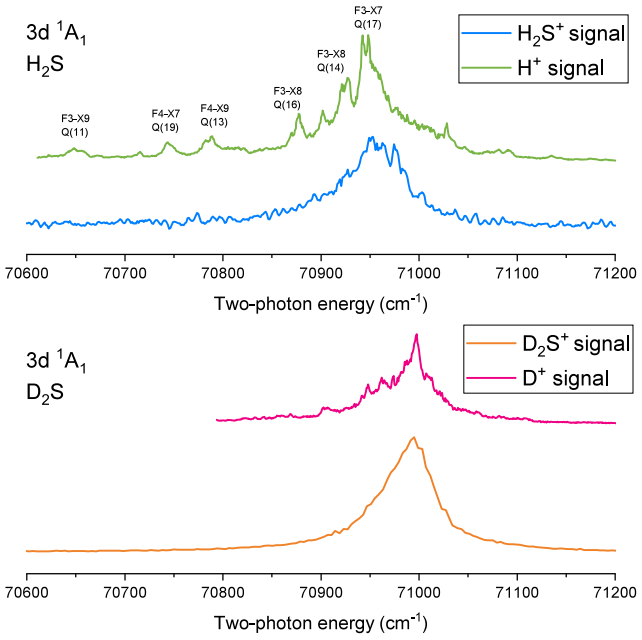


Fig. 1. 2 + 1 REMPI spectra of the H_2S and D_2S parent molecules indicating the two-photon resonances to $3d\ ^1A_1$ electronically excited states used for photolysis in the present study. Besides parent molecule ionization spectra the H^+ and D^+ fragment ion traces are also recorded, showing complex structure. Resonances observed in H^+ spectra are tentatively assigned with EF-X transitions of H_2.

The 1000 cm^{-1} of excess energy in H_2, defined as:

$$E_{excess} = 2 \times h\frac{c}{\lambda_{UV}} - D_0,$$

above dissociation threshold was shown to allow for the formation of quasibound resonances of H_2 at energies up to 500 cm^{-1} above threshold [30,31]. Ro-vibrational level energies of hydrogen sulfide isotopologues have been calculated [40–42] and found in good agreement with experiment [43,44]. The dissociation energy of D_2S in the $S(^1D_2)$ limit can be evaluated with a similar approach outlined in Ref. [38]. The bond dissociation energy of the D-SD bond is determined at 31 999(17) cm^{-1} by Kreis et al. [45], whereas the dissociation energy of the SD radical is determined at 29 660(25) cm^{-1} by Zheng et al. [46]. With the level energy of the $^1D_2$ state of the neutral sulfur atom, the dissociation energy of D_2S at the $S(^1D_2)$ limit is 70 898(30) cm^{-1}.

However, no experimental values are available for the bond dissociation energies of H-SD and D-SH. The dissociation energy of HDS is estimated following the method of determining the bond dissociation energies of water isotopologues by Boyarkin et al. [47]. The isotope effect on the dissociation energy can be expressed in terms of the zero-point energies (E_{ZP}) of the dissociated atomic species. The dissociation energy of HDS to the $S(^1D_2)$ limit is estimated via:

$$D_0(HDS) = D_0(H_2S) + E_{ZP}(H_2S) - E_{ZP}(HDS).$$

Table 1 lists the E_{ZP} for each isotopologue and the estimated D_0 for HDS. E_{ZP} is extracted from global fitting of multiple ro-vibrational bands of the hydrogen sulfide molecule with a Watson's type Hamiltonian [44,48]. Values for E_{ZP} in Table 1 are extracted by fitting the level energies of nine $v_1 + v_2 + v_3 \le 2$ $J_{K_a,K_c} = 0_{00}$ states to a general vibrational energy expression for a triatomic molecule up to the leading order anharmonicity term. The accuracy of this approximation is sufficient for our discussion. The increased zero-point vibrational energies lead to higher dissociation energies for the deuterated species, and hence to lower E_{excess}, which are evaluated from the difference between the two-photon energy at 70 980 cm^{-1} and D_0. These estimated values set the range of resonance energies for the observable quasibound resonances produced from photolysis.

Table 1
Values for zero-point-energy (E_{ZP}), dissociation energy (D_0) with respect to the S($^1D_2$) limit of each hydrogen sulfide isotopologue, and excess energy E_{excess}. All values in cm^{-1}.

Species	E_{ZP} [a]	D_0	E_{excess}
H_2S	3287	69 935[b]	1045
HDS	2844	70 378	602
D_2S	2369	70 898[c]	82

[a]Fitted E_{ZP} from calculated level energies of all $v_1 + v_2 + v_3 \leq 2$ $J_{K_a,K_c} = 0_{00}$ states from Ref. [41].
[b]Experimental value from Ref. [38].
[c]Derived experimental value using the bond dissociation energy of D-SD D_0(D-SD) = 31 999 cm^{-1} from Ref. [45], the dissociation energy of SD radical D_0(S-D) = 29 660 cm^{-1} from Ref. [46] and the level energy of the $^1D_2$ state of the neutral sulfur atom $E(^1D_2)$ = 9238.609 cm^{-1} from the NIST database.

3. Experimental procedures

The experimental configurations for the production of highly excited states in molecular hydrogen and the spectroscopic study of the $F^1\Sigma_g^+$ - $X^1\Sigma_g^+$ transition in a two-laser scheme [49] and a three-laser scheme [27–29,31] scheme were presented before. The measurements on HD and D_2 levels were performed in the simplified two-laser scheme with a frequency-doubled grating-based dye laser (LIOPTEC) for the spectroscopy step. A Doppler-free configuration with counter-propagating beams is employed, while the laser bandwidth is about 0.1 cm^{-1} in the ultraviolet range. Highly excited rovibrational states of HD and D_2 were produced from UV-photolysis and probed via a 2 + 1 REMPI scheme via the F-X transition, without using a dedicated ionization laser. The focused UV pulse is configured in a counter-propagating geometry and overlapped spatially with the molecular beam and photolysis laser. This spectroscopy laser scans over the range of 300–315 nm. By this means many transitions were probed exciting $X^1\Sigma_g^+$ with high v'' to $F^1\Sigma_g^+$ ($v' = 0 - 2$) states, further denoted also as F0, F1 and F2.

Absolute frequency calibration for the spectroscopy step in this two-laser scheme is based on a direct comparison with reference spectra produced via linear absorption spectra of Doppler-broadened resonances in I_2 [50] using the visible output of the dye laser at its fundamental wavelength. The UV-pulse energy of the spectroscopy laser was 1.5–2 mJ per pulse. The pulses of the spectroscopy laser were temporally delayed from pulses from the photolysis laser by 5 ns to avoid ac-Stark contributions by the latter. While some of the measurements in H_2 were performed via this simplified two-laser scheme, part of the measurements of the F-X transitions in H_2 were performed via a more sophisticated three-laser scheme, using a narrowband pulsed-dye-amplification (PDA) system yielding the highest precision [28,29,31].

Experiments were performed on pulsed beams of pure H_2S and D_2S at a stagnation pressure of 2–3 bar. The HDS sample was produced by pre-mixing H_2S and D_2S at a ratio of 3.6 : 1. For an equilibrium constant for the reaction

$$H_2S + D_2S \rightleftharpoons 2\,HDS$$

of 3.88 at room temperature [51], a mixture of H_2S : HDS : D_2S of 3.6 : 1.0 : 0.28 is produced. This mixture is used for the studies of HD spectra.

Signals were recorded by ion detection upon multi-step laser photoionization, involving mass analysis in a time-of-flight (TOF) mass spectrometer, and detection by a micro-channel plate (MCP) with phosphor screen. For the measurements on H_2, the ion optics were triggered at a 80 ns delay from the spectroscopy laser to provide a dc-field-free environment. Both m/z = 1 (H^+) or m/z = 2 (H_2^+) ions are accelerated into the TOF-tube. For HD and D_2, the background ions from the photolysis process outweigh the signal from F-X transitions. Therefore a dc-field of 1.3 kV/cm of opposite polarity was applied to remove prompt ions from the photolysis process. At the accuracy scale of the two-color scheme the induced dc-Stark shift is insignificant. For the HD spectra settings at m/z = 2 (D^+ or H_2^+) and m/z = 3 (HD^+) were employed, where molecular resonances appear in both channels.

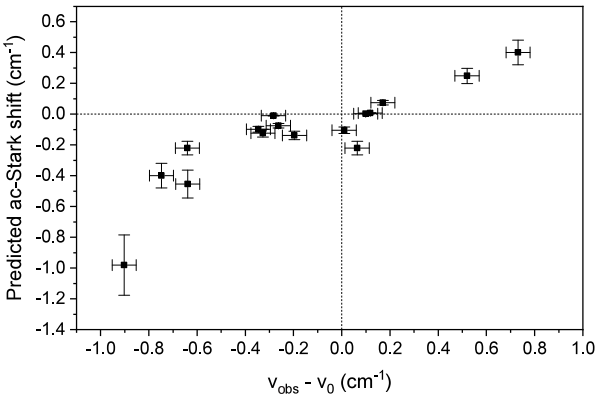


Fig. 2. The predicted ac-Stark shifts for the low-resolution two-color dye-laser measurements, based on measured ac-Stark slope coefficients in the narrowband PDA setup and the power density used in the experiment, plotted against the actually observed ac-Stark shift in the high resolution experiment involving the PDA system.

The major uncertainty in the calibration of F-X two-photon transition frequencies in the two-color scheme stems from the ac-Stark effect induced by the spectroscopy laser. A number of F-X transitions were investigated in the three-laser scheme, using the narrowband PDA laser system and performing intensity-dependent measurements with extrapolation to zero intensity. The latter measurements led to an accuracy of 2×10^{-3} cm^{-1} or 60 MHz for the field-free transition frequencies [27–29,31]. Examples of such spectra for H_2 are presented in the next section. For this subset of 16 high-resolution measurements on H_2 an ac-Stark coefficient was determined from measurements performed at various intensities with extrapolation to zero intensities. The same set of F-X lines was remeasured in the lower resolution two-laser scheme at a laser energy of 2 mJ/pulse. The ac-Stark shifts between the measured frequencies ν_{obs} under these conditions were determined with respect to the zero-intensity values ν_0, while also the expected ac-Stark shifts based on the measured ac-Stark slopes were determined. Results of a comparison between the observed and predicted values, plotted in Fig. 2, demonstrates their correspondence. Taking into account the uncertainties, the correspondence appears to follow a linear behavior; the slope deviating from unity may be ascribed to slightly different focusing conditions and beam geometry in the two- and three-laser schemes.

This result sets a standard for the ac-Stark effect in the F-X transitions, which will be used for estimating uncertainties in the simplified two-color scheme adopted for the HD and D_2 spectroscopies. The root-mean-square of the difference is determined at 0.45 cm^{-1}. Note that in all two-color measurements the laser energy of the UV spectroscopy laser was limited to <2 mJ/pulse. Including a smaller uncertainty related to wavelength calibration results in a value 0.5 cm^{-1}, defining the experimental uncertainty for the measurements performed in the two-color scheme for all isotopologues.

4. Spectroscopy of F-X two-photon transitions

In this section we present the deduced two-photon transition frequencies in the $F^1\Sigma_g^+$ - $X^1\Sigma_g^+$ system of the hydrogen isotopologues. The lines in the two-photon spectra were assigned using several ingredients. Firstly, signal detection was accomplished via the REMPI-TOF method whereby either the molecular fragment ions (H_2^+, HD^+, D_2^+) at masses 2, 3 and 4, or atomic fragments (H^+ or D^+) at masses 1 and 2, were probed.

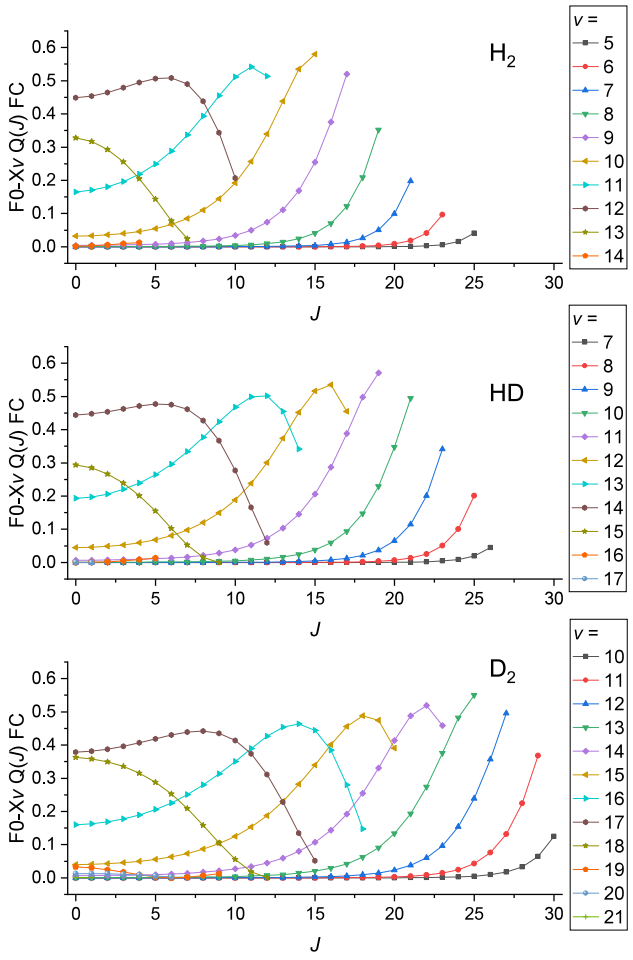


Fig. 3. Calculated Franck–Condon factors for $F^1\Sigma_g^+$ - $X^1\Sigma_g^+$ $(0, v'')$ Q-branch transitions in H_2, HD and D_2.

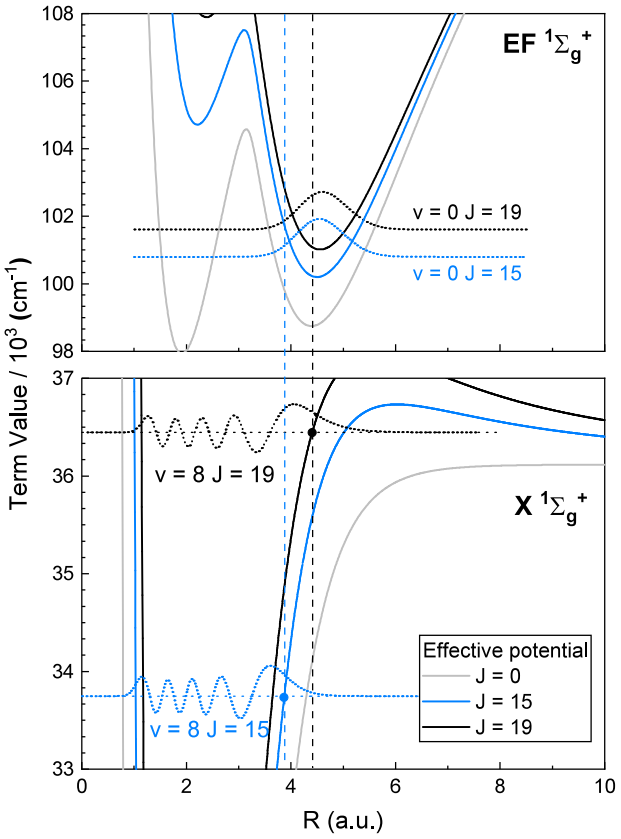


Fig. 4. Effective potential energy curves of $X^1\Sigma_g^+$ and $EF^1\Sigma_g^+$ state at $J = 0, 15, 19$ and radial wavefunctions of $v = 8, J = 15$, $v = 8, J = 19$ in $X^1\Sigma_g^+$ state and $v = 0, J = 15$ and $v = 0, J = 19$ in $F^1\Sigma_g^+$ state. Dots represent the outer classical turning points for $v = 8, J = 15$ (in blue) and $v = 8, J = 19$ (in black) in $X^1\Sigma_g^+$ state. The level energies are drawn for the case of H_2, whereas the potential energy curves pertain to all isotopologues.

Secondly, line intensities were compared to computed Franck–Condon (FC) factors for the various F-X(v', v'') bands. For this purpose FC factors were computed for the relevant bands in the F-X system, for Q-branch transitions in the three isotopologues and as a function of rotational quantum number J. Results for the vibrational progression of F-X$(0, v'')$ bands are presented in Fig. 3.

Fig. 4 shows how the wave density at the classical outer turning point of the $X^1\Sigma_g^+$ state potential provides the overlap with the density on the $F^1\Sigma_g^+$ well. Vibrational wave functions X$(v'' = 5 - 14)$ thus provide access to the F outer well, but the subtle overlap make the FC-factors strongly J-dependent, since the classical outer turning point extends to larger internuclear distances. As a result, it yields an increasing trend in FC factor with increasing J. For moderately high vibrational levels v'', the FC factors increase with the rotational quantum number J for all three isotopologues in the F0-Xv'' progression. For low J values, the wavefunctions of the moderately high v'' vibrational levels in the $X^1\Sigma_g^+$ state with F0-levels are poorly overlapped, producing FC factors smaller than 10^{-5}. The Q-branch transitions with a Franck–Condon factor smaller than 10^{-3} were discarded in the analysis, as they may be confused with the weaker S-/O-side-branch lines, which are known to be much weaker than the main Q-branch lines in the $EF^1\Sigma_g^+$-$X^1\Sigma_g^+$ two-photon transition in molecular hydrogen [24].

Thirdly, combination differences occurring between lines in the spectra were employed. Combination differences exist between S-/Q-/O-lines, as well as between vibrational splittings in the X-ground and F-excited states. In the analysis the level energies for the $X^1\Sigma_g^+(v, J)$ ground electronic state as obtained from H2SPECTRE [52], accurate to within 10^{-3} cm^{-1}, are considered to be exact for the purpose of assignment.

As for a fourth ingredient the level energies of $F^1\Sigma_g^+$ rovibrational states were computed via ab initio methods including non-adiabatic effects. These calculations use improved BO potential energy curves for excited states of molecular hydrogen that have recently become available [53]. The computational methods and results will be presented in Section 6. Alongside multi-channel quantum defect (MQDT) calculations [9] were also used to compare with experimental results.

In a few examples, an independent photoionization laser was used for recording autoionization spectra aimed at assigning the rotational quantum numbers of the F-X two-photon transitions Some examples were presented previously [27–29,31]. However, this additional method is limited to the use of the three-color scheme and too time-consuming to apply it to large numbers of spectral lines.

4.1. H_2

Several portions of the 2+1 REMPI spectra of the $F^1\Sigma_g^+X^1\Sigma_g^+$ system in H_2 were presented in previous publications [29,31]. Most of the resonances observed were concentrated between 64 400–65 200 cm^{-1}, covering the range of excitations from X12, X13 and X14 levels to F0 and F1 upper levels. Almost all the transitions observed in H_2^+ ion spectra were also observed via H^+ detection.

In Fig. 5 an overview spectrum of the F-X two-photon transitions, as measured via the two-laser scheme, is shown for the region 64 700–65 600 cm^{-1}. Here, three lines are indicated that originate in the same X$(v = 8, J = 19)$ ground level. The assignment yields direct information

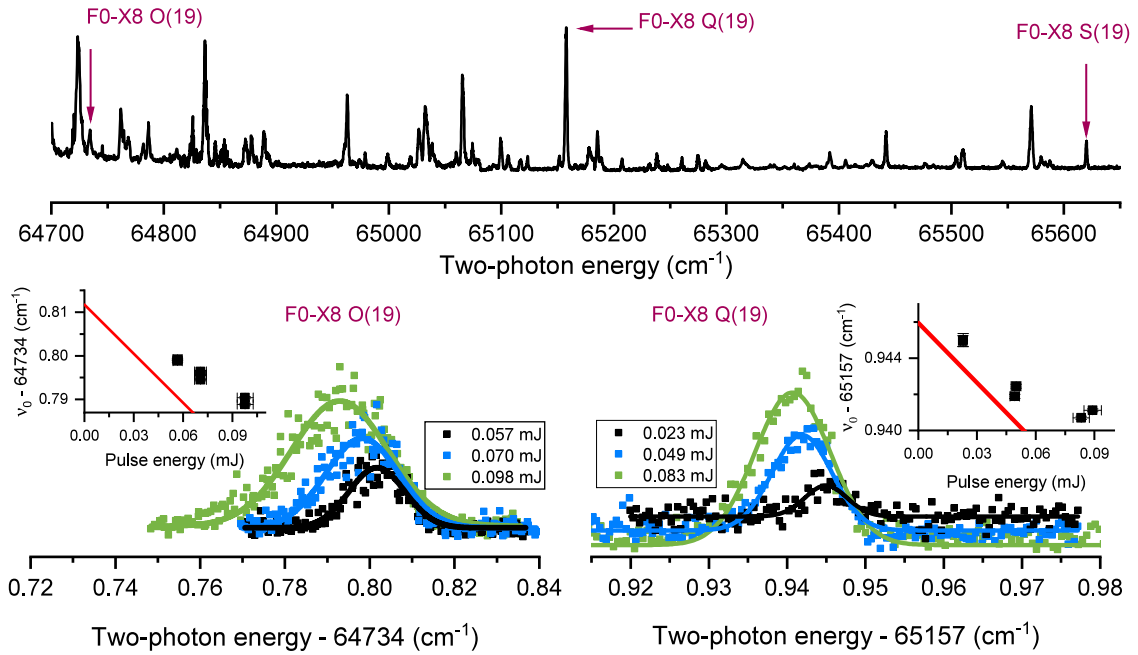


Fig. 5. Spectra of F-X two-photon transitions in H_2 produced via photolysis of H_2S. Upper panel: Overview low-resolution spectrum recorded via 2 + 1 REMPI in the two-color scheme. Here all three two-photon allowed transitions from $X^1\Sigma_g^+$ $v = 8, J = 19$ to F0 states are observed. Lower panel: High resolution spectra of two-photon F-X transitions recorded in the three-color scheme, also involving an ac-Stark analysis and extrapolation to zero-intensity of the spectroscopy laser.

Table 2
Experimentally determined two-photon transition frequencies in the F-X system of H_2 with uncertainties given in brackets. The ac-Stark slope coefficients are given in units of cm^{-1}/mJ.

Transition	ν_0 (cm^{-1})	ac-Stark coefficient
F0-X7 Q(21)	65 441.358 (1)	0.12
F0-X8 Q(19)	65 157.941 (2)	−0.06
F0-X8 S(19)	65 619.860 (1)	0.00
F0-X8 O(19)	64 734.810 (1)	−0.23
F0-X9 Q(17)	64 837.297 (2)	−0.20
F0-X10 Q(15)	64 493.240 (1)	0.20
F0-X8 Q(17)	66 044.705 (1)	0.00
F0-X9 Q(15)	65 571.906 (2)	−0.49
F0-X9 S(15)	65 954.451 (1)	−0.05
F0-X13 Q(5)	63 771.984 (2)	−0.05
F0-X13 Q(3)	63 905.931 (2)	−0.11
F0-X13 Q(1)	63 993.792 (2)	−0.07
F0-X12 Q(4)	64 781.678 (1)	−0.11
F1-X13 Q(0)	65 207.533 (5)	−0.00
F1-X13 Q(1)	65 188.589 (5)	0.04
F1-X13 Q(2)	65 151.813 (5)	−0.04

on the energy separations between rotational levels in the F0 level. In total 113 lines were observed and assigned in the F(v')-X(v'') system of H_2 through measurement of H^+ ion spectra, while 44 lines were observed via H_2^+ ion detection. In total 118 individual transitions were assigned, in excitation from X($v'' = 6 - 14$) levels to F($v'' = 0 - 2$). Some 32 and 10 transitions were observed probing F1 and F2 excited vibrations. This coverage of quantum states was limited by the scanning range adopted for the spectroscopy laser.

In the lower panels of Fig. 5 two high-resolution spectra are displayed as recorded in the three-laser scheme exploiting the narrowband PDA system for the spectroscopy step. A list of results obtained via this high-resolution scheme is presented in Table 2. For the lines listed the ac-Stark shift was quantitatively analyzed by performing measurements at differing intensities leading to a determination of ac-Stark slope coefficients, as shown in the insets of Fig. 5. The values for the extracted coefficients are given in the Table as experimental parameters in units of cm^{-1}/mJ. In principle these values could be converted to proper power densities in units of ac-Stark shifts in MHz per MW/cm^2, but in view of the large uncertainties in the focal spot size no such conversion will be made and the ac-Stark slope coefficients will only be given in measured units of cm^{-1}/mJ. The regularity of data points in Fig. 5 indicates that the relative values display a convincing degree of consistency.

The ac-Stark slope coefficients appear to exhibit positive and negative values for the different lines. The coefficients reflect the entire level structure of the hydrogen molecule since they involve field-induced couplings over all quantum levels in molecular hydrogen [27]. As such the ac-Stark effect may be considered a high-order moment of the quantum level structure of a molecule. No quantitative theory for these ac-Stark shifts and slope coefficients has been developed. Development of such a theory, tested against experimental parameters would provide information on dynamical polarizabilities of the hydrogen molecule [27]. In the literature values have been presented for ac-Stark slope coefficients over several decades, in many cases focusing on the EF-X two-photon transition in H_2 [27,49,54–57]. All resulting values are of order few MHz per MW/cm^2, but they appear randomly distributed. The listing of the present large data set on slope coefficients may be useful for benchmarking future theories on the phenomenon.

In previous studies [30,31], five quasibound resonances on the X-ground state potential have been observed through F0-X transitions: (v, J) = (11,13), (10,15), (9,17), (8,19), (7,21). In the present two-color spectra, four of these quasibound resonances, except for (11,13), are again observed in both F0-X and F1-X Q-branch transitions. The absence of the (11,13) quasibound resonance in the two-color spectra may be due to its short 1.6 ns lifetime. In the present study an additional quasibound resonance (6,23) is found through the F0-X6 Q(23) transition at 65 678.80 cm^{-1} as shown in Fig. 6. The calculated excess energy of the (6,23) resonance is 767.79 cm^{-1}, while its lifetime is about 30 μs [58]. As discussed in Section 2, (6,23) is energetically favorable to be produced upon photolysis of H_2S at 281.8 nm. Through the combination difference with the F0-X7 S(21) transition, the ground state interval between (7,21) and (6,23) is 261.15 cm^{-1}, while the calculated value is 261.86 cm^{-1}.

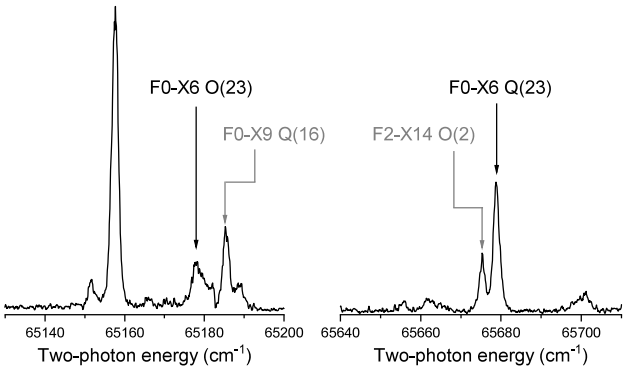


Fig. 6. Observation of the quasibound resonance X(v, J) = (6,23) excited via the F0-X6 Q(23) and the weak F0-X6 O(23) two-photon transitions, using H^+ ion detection.

The large set of data on the low-resolution $F^1\Sigma_g^+ X^1\Sigma_g^+$ two-photon transition frequencies in H_2 are listed in Table 11 in Appendix. For these data the major uncertainty derives from the estimated ac-Stark effect.

4.2. HD

Spectra of HD were recorded using a premixture of H_2S/HDS/D_2S gases for the molecular beam. The (2 + 1) REMPI spectra of the $F^1\Sigma_g^+$ - $X^1\Sigma_g^+$ transitions were recorded through H^+, D^+ and HD^+ signal detection. In the REMPI spectra of the hydrogen molecule often both parent molecular ions as well as fragment atomic ions are observed, where the latter can be produced via various pathways [59]. In the present case the H^+ detected spectra from HD resonances were overwhelmed by the (2 + 1) REMPI signal from H_2 produced from the gas mixture with over 70% of H_2S. The $m/z = 2$ signals are produced by H_2^+ ions from H_2 and D^+ from HD or D_2. Fortunately, these H_2^+ signals from H_2 are sparse in the current scanning range, while the D^+ signals from D_2 are of low intensity as only 5% of D_2S is contained in the precursor mixture. For the analysis of F-X resonances in HD (2 + 1) REMPI spectra are recorded in separate scans with the ion-mass analyzed set at $m/z = 2$ (probing D^+ and H_2^+ ions) and at $m/z = 3$ (probing HD^+). In contrast to the case of H_2S large non-resonant background ion signals were detected from the photolysis process. In order to mitigate this and to increase the signal-to-background ratio for the HD spectra, a 1.3 kV/cm dc-field was applied to remove prompt ions.

Fig. 7 shows the HD spectrum in the scan region 63 800–64 800 cm^{-1} for both $m/z = 2$ and $m/z = 3$ ion traces. Many transitions probed at $m/z = 2$ can be assigned to H_2 as indicated in the top panel, while a good fraction of the lines is assigned to HD resonances. For HD mostly lines in the F0-X13, F0-X14 and F1-X15 bands are identified. In total 97 lines and 108 lines were observed and assigned in the HD F-X transitions through D^+ and HD^+ ion spectra respectively. In total 129 individual transitions were labeled with X($v'' = 7 - 17$) levels to F($v' = 0 - 3$) levels. Similar as in the case of H_2, the majority of transitions were assigned as F0-X, amounting to 91 lines observed. Only 10 transitions to F($v' = 2, 3$) levels were assigned in view of the relatively small Franck–Condon factors, compared to F0-X and F1-X systems. A complete list of transition frequencies in HD is presented in Table 12 in Appendix.

4.3. D_2

The quality of D_2 spectra is inferior to those of the other isotopologues, even though pure D_2S was used as precursor in the photolysis. The photolysis of D_2S was found to generate large amounts of prompt ions, which were partly removed by applying an opposite polarity dc-field, but still the remaining background lowers the sensitivity of the (2 + 1) REMPI signals for D_2. The scanning range of the spectroscopy laser also covers several absorption bands of the D_2S parent molecule, for example the $4p\ ^1A_2$ band at 315 nm and vibronic bands at 302 and 310 nm. Hence the spectroscopy lasers also cause photolysis and the production of various fragment ions. Reducing the pulse energy of the

Table 3
Derived experimental level energies of F0 and F1 states in H_2 measured in the high resolution setup using the PDA laser system. A comparison is made with data from FT-emission spectra [22], results from MQDT calculations [9] as well as from the present non-adiabatic calculations (NA). All values in cm^{-1}.

	J	Exp.	FT [22]	MQDT [9]	NA
F0	0	99 363.805(5)	99 363.8875(4)	99 365.22	99 363.50
	1	99 376.044(4)	99 376.0474(4)	99 377.46	99 375.75
	2	99 400.504(4)	99 400.512(1)	99 401.92	99 400.24
	3	99 437.160(4)	99 437.1665(5)	99 438.57	99 436.94
	4	99 485.964(4)	99 485.971(3)	99 487.37	99 485.79
	5	99 546.859(5)	99 546.868(1)	99 548.26	99 546.76
	6	99 619.784(6)	–	99 621.16	99 619.75
	7	99 704.622(3)	–	99 706.04	99 704.68
	9	99 909.63(2)	–	99 911.06	99 909.93
	11	100 160.993(5)	–	100 162.41	100 161.54
	13	100 457.50(2)	–	100 458.95	100 458.33
	15	100 797.766(4)	–	100 799.23	100 798.94
	17	101 180.310(4)	–	101 181.92	101 181.84
	19	101 603.441(5)	–	101 604.93	101 605.35
	21	102 065.360(4)	–	–	102 067.66
F1	0	100 558.853(5)	100 558.851(1)	100 563.13	100 558.95
	1	100 570.841(5)	100 570.843(3)	100 575.13	100 570.58
	2	100 594.800(5)	100 594.8070(6)	100 599.11	100 594.57
	4	100 678.50(2)	100 678.510(1)	100 682.87	100 678.37

Table 4
Derived experimental level energies of F0, F1 and F2 states in H_2 measured via the lower accuracy two-laser scheme. The accuracy of the level energies of 0.5 cm^{-1} is limited mainly by the (estimated) ac-Stark effect. A comparison is made with results from the present non-adiabatic calculations (NA) and with results from MQDT calculations [9]. All values in cm^{-1}.

State	J	Exp.	NA. Calc.	MQDT [9]
F0	8	99 801.2(5)	99 801.44	99 802.69
	10	100 029.4(5)	100 030.01	100 031.02
	12	100 303.9(5)	100 304.37	100 305.16
	14	100 622.4(5)	100 623.25	100 623.71
	16	100 984.0(5)	100 985.21	100 985.51
	18	101 386.2(5)	101 388.63	101 388.55
	20	101 829.5(5)	101 831.78	–
	23	102 564.3(5)	102 566.84	–
F1	3	100 629.8(5)	100 630.52	100 635.04
	5	100 737.5(5)	100 738.06	100 742.53
	6[a]	100 811.6(5)	100 809.51	100 813.97
	7	100 892.2(5)	100 892.66	100 897.02
	8	100 986.8(5)	100 987.29	100 991.72
	9	101 093.5(5)	101 093.39	101 097.75
	10	101 210.7(5)	101 210.78	101 215.08
	12	101 477.7(5)	101 478.82	101 483.13
	13	101 628.4(5)	101 629.14	101 633.31
	14	101 789.0(5)	101 790.09	101 794.16
	15	101 960.1(5)	101 961.46	101 965.41
	16	102 141.8(5)	102 143.06	102 147.13
	17	102 333.1(5)	102 334.68	102 338.46
	19	102 745.1(5)	102 747.07	102 750.68
	21	103 194.4(5)	103 196.79	–
F2	0	101 698.5(5)	101 698.74	101 703.92
	1	101 710.9(5)	101 710.65	101 715.79
	2	101 734.6(5)	101 734.87	101 739.80
	3	101 768.4(5)	101 768.45	101 773.47
	5	101 874.3(5)	101 874.84	101 879.68
	6	101 943.2(5)	101 945.09	101 949.82
	7	102 026.8(5)	102 026.74	102 031.26
	9	102 224.7(5)	102 223.76	102 227.83
	11	102 465.0(5)	102 464.72	102 468.22

[a]Tentative assignment.

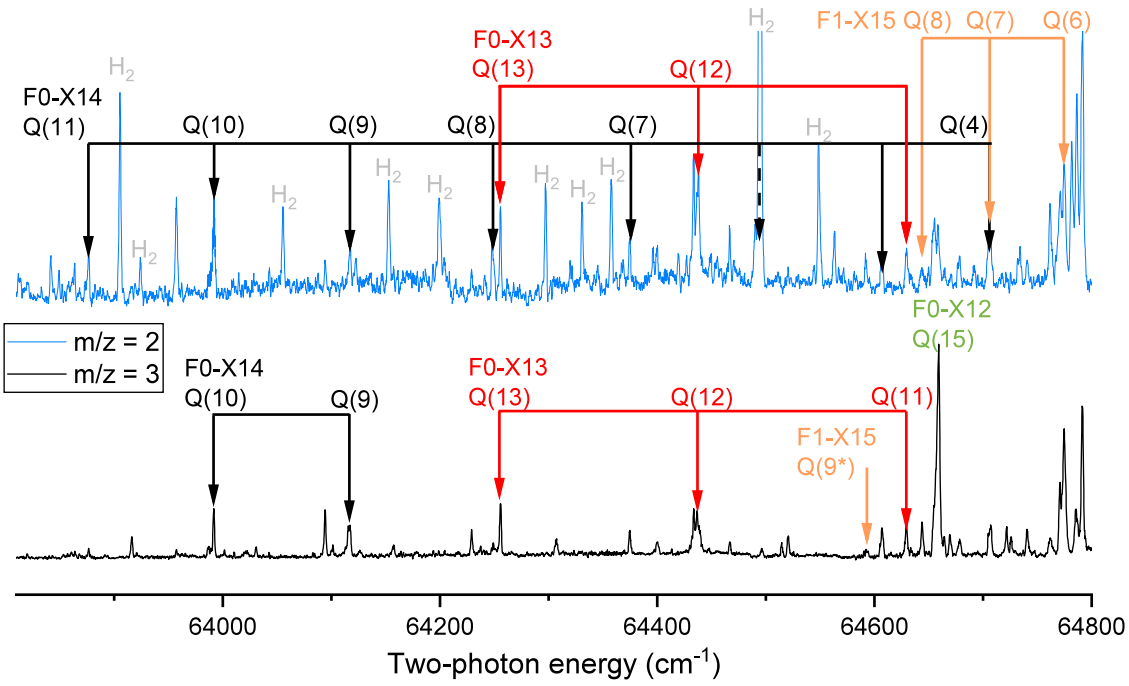


Fig. 7. Overview of two-photon spectra in the F-X system in for the HD photofragment as recorded in the two-color laser scheme with the $H_2S/HDS/D_2S$ premixture before photolysis. The upper panel is the spectrum for $m/z = 2$ (D^+ and H_2^+) detection; the lower panel for $m/z = 3$ detection (HD^+).

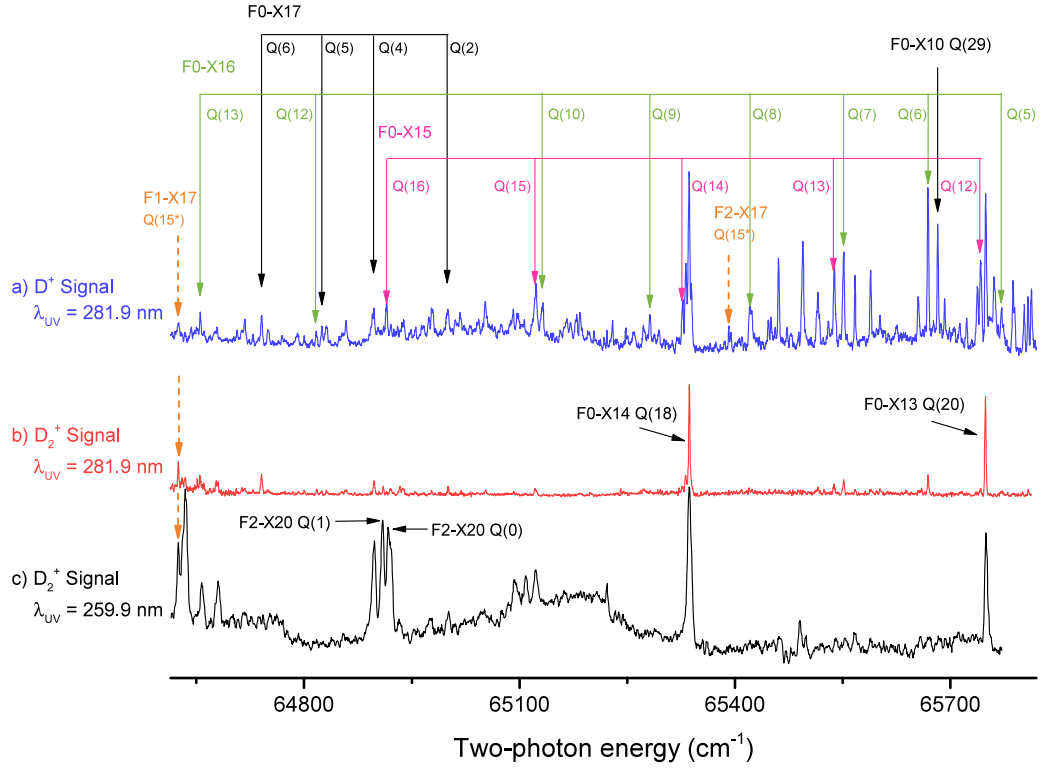


Fig. 8. Overview spectra of D_2 resonances in the F-X system upon photolysis of D_2S for the various choices of photolysis wavelengths and fragment ion detection as indicated. The transitions probing the ($v = 17$, $J = 15$) quasi-bound resonance in D_2 are indicated by a dashed arrow.

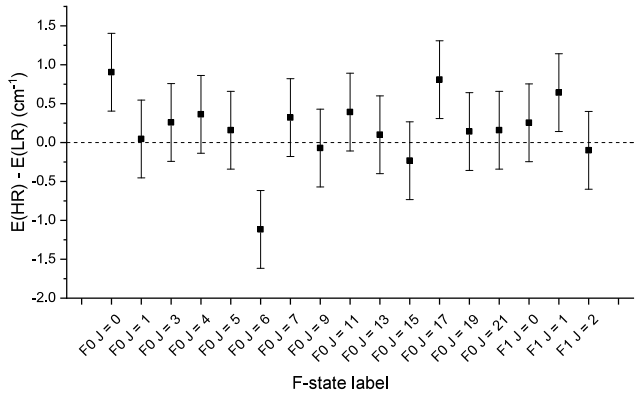


Fig. 9. Difference between derived level energies for levels in the $F^1\Sigma_g^+$ state in H_2 measured via the high resolution setup, resulting in E(HR), and via the low resolution two-color setup, resulting in values E(LR).

Table 5
Derived experimental level energies of F0 states in HD measured in this work. A comparison is made with the present non-adiabatic calculations (NA). All values in cm^{-1}.

State	J	Exp.	NA. Calc.
F0	0	99 577.5(5)	99 576.54
	1	99 586.4(5)	99 585.74
	2	99 604.3(5)	99 604.15
	3	99 632.1(5)	99 631.73
	4	99 668.8(5)	99 668.47
	5	99 714.0(5)	99 714.35
	6	99 769.7(5)	99 769.28
	7	99 833.2(5)	99 833.26
	8	99 907.4(5)	99 906.21
	9	99 987.9(5)	99 988.06
	10	100 078.5(5)	100 078.75
	11	100 178.1(5)	100 178.20
	12	100 286.4(5)	100 286.31
	13	100 402.9(5)	100 402.99
	14	100 527.5(5)	100 528.14
	15	100 661.1(5)	100 661.66
	16	100 803.0(5)	100 803.42
	17	100 953.5(5)	100 953.31
	18	101 110.5(5)	101 111.21
	19	101 276.0(5)	101 276.98
	20	101 449.4(5)	101 450.48
	21	101 630.6(5)	101 631.58
	22	101 818.5(5)	101 820.14
	23	102 014.9(5)	102 015.99
	24	102 217.4(5)	102 218.98
	26	102 643.1(5)	102 645.78

spectroscopy laser was not an option since the 2 + 1 REMPI signals of D_2 would lower the signal-to-noise by ratio too much.

In Fig. 8 spectra of F-X two-photon transitions in the D_2 molecule are presented. Three different recordings were performed over the spectral range 64 650–65 750 cm^{-1}. With the dissociation laser set at λ_{UV} = 281.8 nm many resonances were observed for detection in the D^+ signal channel ($m/z = 2$). This spectrum shows the progressions F0-X(v'') for $v'' = 15 - 17$. For detection in the D_2^+ channel ($m/z = 4$) only a few marked resonances were observed in this energy range.

In total 93 lines were observed via D^+ ion detection and 39 lines via D_2^+ ion detection. In total 112 individual transitions were assigned to F-X two-photon transitions combining X($v'' = 10 - 20$) ground levels and F($v' = 0 - 4$) excited levels. The spectra in the D_2 measurement appear denser than those for H_2 and HD due to its larger moment of inertia. This density limits the assignment of transitions in regions where unresolved bands are observed at poor signal-to-noise ratio. The fact that the lines observed via D_2^+ detection are erratically distributed may point to a decisive influence of the ionization step, whereby signal is only enhanced for some random lines, where the ionization step

Table 6
Derived experimental level energies of F1 states in HD measured in this work. A comparison is made with the present non-adiabatic calculations (NA). All values in cm^{-1}.

State	J	Exp.	NA. Calc.
F1	2	100 645.7(5)	100 645.39
	3	100 673.1(5)	100 672.47
	4[a]	100 706.0(5)	100 708.55
	5	100 753.9(5)	100 753.57
	6	100 807.5(5)	100 807.50
	7	100 870.9(5)	100 870.28
	8	100 942.6(5)	100 941.86
	9	101 022.1(5)	101 022.16
	12	101 314.9(5)	101 314.57
	13	101 429.1(5)	101 428.90
	14	101 552.9(5)	101 551.50
	15	101 681.6(5)	101 682.25
	16	101 821.1(5)	101 821.03
	17	101 967.4(5)	101 967.72
	18	102 123.3(5)	102 122.19
	19	102 283.9(5)	102 284.31
	22	102 816.3(5)	102 815.11

[a]Tentative assignment.

Table 7
Derived experimental level energies of F2 and F3 states in HD measured in this work. A comparison is made with the present non-adiabatic calculations (NA). All values in cm^{-1}.

State	J	Exp.	NA. Calc.
F2	4	101 707.9(5)	101 708.55
	5	101 753.0(5)	101 753.57
	7	101 868.3(5)	101 867.56
	8	101 937.5(5)	101 937.25
	10	102 102.9(5)	102 103.56
	14	102 534.9(5)	102 535.81
	16	102 799.9(5)	102 800.02
F3	0	102 579.7(5)	102 577.10
	1	102 586.7(5)	102 585.94

matches a transition from the F-state to an autoionizing resonance in the two-color scheme.

In a third spectrum the photolysis laser was moved to λ_{UV} = 259.9 nm, while the ion detection was kept at the D_2^+ channel. Some strong transitions for photolysis at λ_{UV} = 281.8 nm are reproduced, while some additional resonances probing lines in the F2-X20 band appear in the spectrum.

From Table 1, the estimated E_{excess} for photolysis of D_2S at λ_{UV} = 281.8 nm is estimated at 82 cm^{-1}, which limits the number of quasi-bound or shape resonances to form. In the present study the (v, J) = (17,15) resonance was observed in Q-branch transitions F1-X17 Q(15) at 64 624.84 cm^{-1} and F2-X17 Q(15) at 65 446.28 cm^{-1}. Here the photolysis wavelength of 281.8 nm was used. For measurements of D_2S photolysis at 259.9 nm with E_{excess} > 6000 cm^{-1}, the F1-X17 Q(15) transition, probing this quasi-bound resonance, was also observed. Combining these experimental results with a calculation of F-level energies (see below) it can be concluded that the $(17, 15)$ resonance is at a collision energy of 31 cm^{-1}, well below the accessible excess energy from photolysis. We conclude that there is firm evidence for the assignment of the ($v = 17$, $J = 15$) quasi-bound resonance in D_2.

The observed two-photon transition frequencies in the F-X system of D_2 are presented in Table 13 in Appendix.

5. F-level energies

The term values for the $F^1\Sigma_g^+$ outer well rovibrational levels, relative to the $X^1\Sigma_g^+(v = 0, J = 0)$ ground level, can be derived by adding the presently measured two-photon transition frequencies to the calculated term values of ro-vibrational $X^1\Sigma_g^+$ levels [35,36]. In this procedure a

Table 8
Derived experimental level energies of F0 states in D_2 measured in this work. A comparison is made with the present non-adiabatic calculations (NA) and with the results from FT-emission studies [23]. All values in cm^{-1}.

State	J	Exp.	NA. Calc.	Ref. [23].
F0	1	99 835.2(5)	99 834.96	99 835.190(5)
	2	99 846.6(5)	99 847.26	99 847.581(5)
	4	99 890.1(5)	99 890.27	99 890.577(5)
	5	99 921.4(5)	99 920.96	99 921.241(5)
	6	99 958.1(5)	99 957.73	
	7	99 999.9(5)	100 000.60	
	8	100 049.7(5)	100 049.50	
	9	100 104.1(5)	100 104.42	
	10	100 165.0(5)	100 165.33	
	11	100 231.9(5)	100 232.19	
	12	100 305.4(5)	100 304.96	
	13	100 384.0(5)	100 383.60	
	14	100 466.5(5)	100 468.06	
	15	100 558.9(5)	100 558.29	
	16	100 653.5(5)	100 654.24	
	17	100 755.7(5)	100 755.86	
	18	100 862.9(5)	100 863.08	
	19	100 975.4(5)	100 975.84	
	20	101 093.7(5)	101 094.10	
	21	101 217.9(5)	101 217.77	
	22	101 347.6(5)	101 346.78	
	23	101 481.2(5)	101 481.07	
	24[a]	101 618.7(5)	101 620.57	
	26	101 915.7(5)	101 914.87	
	27	102 068.8(5)	102 069.51	
	29	102 392.3(5)	102 393.38	

[a]Tentative assignment.

Table 9
Derived experimental level energies of F1 states in D_2 measured in this work. A comparison is made with the present non-adiabatic calculations (NA) and with the results from FT-emission studies [23]. All values in cm^{-1}.

State	J	Exp.	NA. Calc.	Ref. [23].
F1	0	100 687.3(5)	100 685.92	100 686.239(5)
	2	100 703.5(5)	100 704.10	100 704.409(5)
	3	100 721.1(5)	100 722.28	100 722.567(5)
	4	100 746.9(5)	100 746.46	100 746.741(5)
	5	100 777.1(5)	100 776.68	100 776.969(5)
	6	100 812.3(5)	100 812.90	100 814.897(10)
	7	100 856.0(5)	100 855.10	
	8	100 903.4(5)	100 903.24	
	10	101 016.7(5)	101 017.27	
	11	101 082.7(5)	101 083.07	
	12	101 155.0(5)	101 154.68	
	13	101 231.8(5)	101 232.05	
	14	101 313.4(5)	101 315.13	
	15	101 403.9(5)	101 403.87	
	16	101 498.8(5)	101 498.23	
	17	101 598.6(5)	101 598.13	
	19	101 813.0(5)	101 814.36	
	20	101 930.1(5)	101 930.55	
	21	102 051.9(5)	102 052.03	
	22	102 179.0(5)	102 178.74	
	23	102 310.0(5)	102 310.61	
	24	102 447.2(5)	102 447.55	
	26	102 735.5(5)	102 736.36	
	29	103 204.8(5)	103 205.68	

statistical and weighted average is taken over all calibrated two-photon lines probing the same upper level in the $F^1\Sigma_g^+$ state. A similar approach was followed for the determination of level energies for high rotational states in the E0–E3 inner well states with J up to 19 [9]. The accuracy of the X(v, J) ground state levels is about 10^{-3} cm^{-1}, for some levels at low v and J even as accurate as 10^{-5} cm^{-1} [60,61]. The accuracy for the highest X(v) levels was experimentally tested via measurement of combination differences for $v'' = 13, 14$ [29].

Table 3 lists the thus derived $F^1\Sigma_g^+$ state term values in H_2 as obtained from the accurate three-laser experiments employing the narrow

Table 10
Derived experimental level energies of F2, F3 and F4 states in D_2 measured in this work. A comparison is made with the present non-adiabatic calculations (NA) and with the results from FT-emission studies [23]. All values in cm^{-1}.

State	J	Exp.	NA. Calc.	Ref. [23].
F2	0	101 515.1(5)	101 515.76	101 516.074(5)
	2	101 534.3(5)	101 533.69	101 533.990(5)
	3	101 549.1(5)	101 551.60	101 551.890(2)
	4	101 575.4(5)	101 575.46	101 575.746(2)
	5	101 604.1(5)	101 605.60	101 605.675(2)
	11	101 907.9(5)	101 907.22	
	12	101 978.1(5)	101 977.75	
	15	102 225.6(5)	102 223.10	
F3	8	102 529.5(5)	102 529.72	
F4	7	103 254.7(5)	103 254.90	

PDA system for the spectroscopy step, while also the ac-Stark effect was addressed quantitatively. Such high-accuracy values are determined for F0 and rotational quantum numbers $J = 0 - 21$, restricted to low J and for higher-J levels to the odd J levels in ortho-H_2. In addition four term values in F1 were determined for low-J values. Table 3 also includes a comparison with experimentally determined energies of F0 and F1 levels from Fourier-transform emission studies [22] as well as with a multi-channel quantum-defect (MQDT) calculation for the same levels [57] up to $J = 19$. The differences with the results from the FT-emission data [22] are all less than 0.01 cm^{-1} and at the level of the combined accuracies, with the exception of the F0($J = 0$) level where the difference is much larger amounting to 0.08 cm^{-1}.

In addition to the high-accuracy data extracted from the three-color PDA-based measurements, level energies of some missing rovibrational levels in F0 and F1 states, as well as for F2 were derived from the lower resolution two-color laser measurements. Those results are presented in Table 4. The energies for the F-levels are obtained by averaging over results of measurements of multiple lines in the F-X system. For a subset of 16 levels results for F-level energies as obtained from the high-resolution three-color scheme are compared to results as obtained form the low-resolution two-color laser excitation scheme. The deviations, as plotted in Fig. 9, show that those fall again statistically within the 1σ uncertainty of 0.5 cm^{-1}. This proves that the methods of the two-color laser scheme yield F-level energies at an accuracy of 0.5 cm^{-1}. This sets the standard uncertainty for F-levels also in HD and D_2 isotopologues.

Similar results for $F^1\Sigma_g^+$ level energies in HD are presented in Table 5 for the F0 manifold up to $J = 26$, in Table 6 for the F1 manifold up to $J = 22$, while in Table 7 some additional levels pertaining to F2 and F3 are listed.

Results for experimental $F^1\Sigma_g^+$ level energies in D_2 are presented in Table 8 for the F0 manifold observed up to $J = 29$, in Table 9 for the F1 manifold also observed up to $J = 29$, while in Table 10 some levels pertaining to the F2, F3 and F4 manifolds are listed.

6. Non-adiabatic calculations

To assist the assignment of the 2 + 1 REMPI spectra for the F-X system, theoretical evaluations for the level energies of $F^1\Sigma_g^+$ rovibrational levels are used, besides those of the highly accurate levels of the $X^1\Sigma_g^+$ ground state available from non-adiabatic perturbation theory (NAPT) from the H2SPECTRE program suite [35,52]. The latter are accurate to 10^{-3} cm^{-1}, and can be considered exact for the purpose of comparison with the present experimental data.

The accuracy of ab initio computation of excited state level energies has not reached the same level of accuracy as those for the ground state. However, an extremely accurate calculation was performed in a pre-Born–Oppenheimer framework including relativistic and high-order QED-corrections finding excellent agreement within 0.001 cm^{-1} for the $J \leq 5$ levels in the $E^1\Sigma_g^+$ inner well state [62]. The Dressler group had previously computed accurate values for the level energies

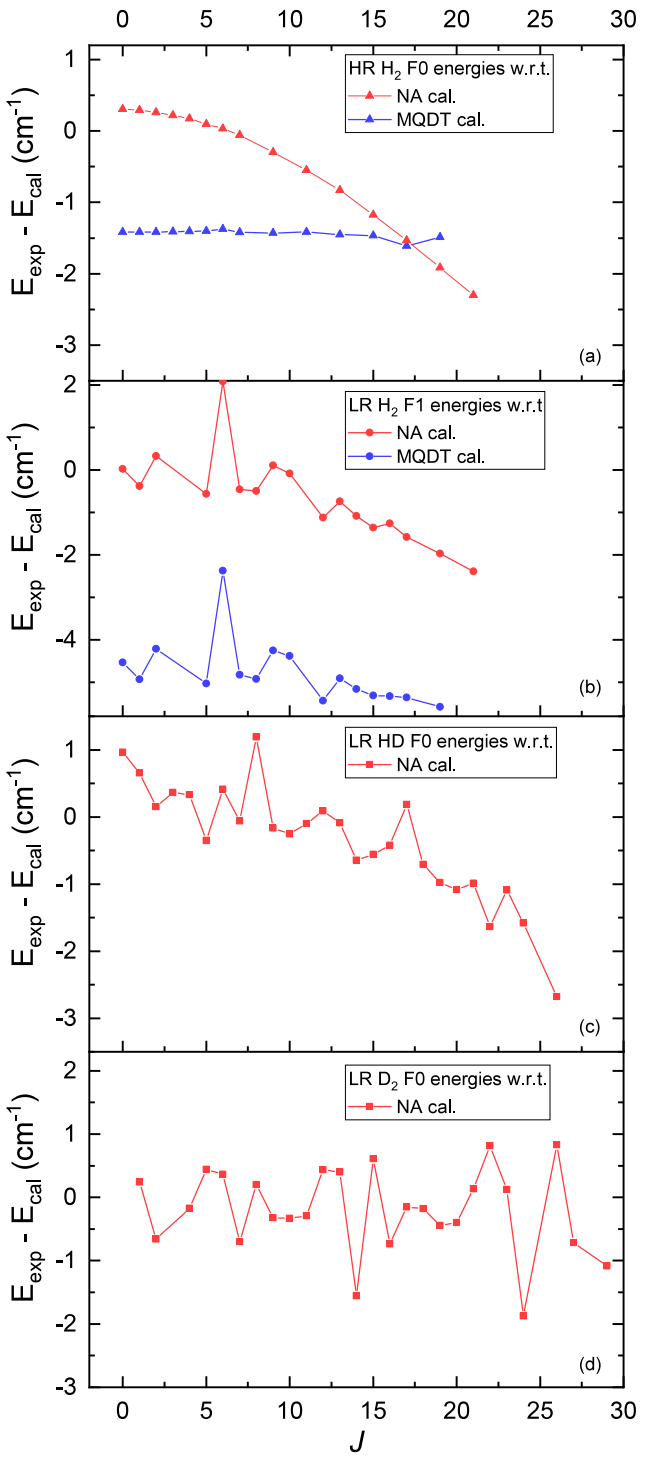


Fig. 10. Comparison of the experimentally determined level energies in the various hydrogen isotopologues with calculated values. (a) Experimental values for the F0 levels in H_2 as obtained via the high-resolution (HR) setup with the three-laser scheme, compared with values from the present nonadiabatic calculations and with values from MQDT calculations [9]; (b) Experimental values for the F1 levels in H_2 obtained via the low-resolution setup with the two-color laser scheme, compared with nonadiabatic and MQDT calculations; Experimental F0 levels in HD (c) and D_2 (d) compared with nonadiabatic calculations.

in a non-adiabatic framework [4,33]. These calculations had reached sub-cm^{-1} accuracy, and included levels in the $F^1\Sigma_g^+$ outer well, but the results were limited to low-J values.

Table 11
H_2 linelist.

v_F	v_X	Line	Freq.	v_F	v_X	Line	Freq.
0	6	O(23)	65 178.27	0	6	Q(23)	65 678.80
0	7	Q(19)	66 470.39	0	7	Q(20)	65 933.05
0	7	O(21)	64 978.92	0	7	Q(21)	65 441.88
0	7	S(21)	65 939.95	0	8	O(17)	65 662.00
0	8	Q(17)	66 044.80	0	8	Q(18)	65 579.83
0	8	O(19)	64 734.17	0	8	Q(19)	65 157.61
0	8	S(19)	65 619.98	0	9	Q(13)	66 409.96
0	9	Q(14)	65 983.54	0	9	O(15)	65 231.64
0	9	Q(15)	65 571.25	0	9	S(15)	65 954.46
0	9	Q(16)	65 185.48	0	9	S(16)	65 587.59
0	9	O(17)	64 456.20	0	9	Q(17)	64 836.51
0	9	S(17)	65 260.54	0	10	Q(9)	66 400.53
0	10	Q(10)	66 067.28	0	10	O(11)	65 476.88
0	10	Q(11)	65 728.25	0	10	S(11)	66 024.40
0	10	O(12)	65 116.96	0	10	Q(12)	65 392.15
0	10	O(13)	64 768.88	0	10	Q(13)	65 065.84
0	10	S(13)	65 406.04	0	10	O(14)	64 443.43
0	10	Q(14)	64 761.93	0	10	S(14)	65 123.36
0	10	O(15)	64 152.75	0	10	Q(15)	64 493.97
0	10	S(15)	64 872.86	0	11	Q(5)	65 931.85
0	11	Q(7)	65 510.35	0	11	O(8)	65 093.42
0	11	Q(8)	65 274.82	0	11	S(9)	65 281.71
0	11	Q(10)	64 786.26	0	11	S(10)	65 059.98
0	11	O(11)	64 297.61	0	11	Q(11)	64 548.96
0	11	S(11)	64 845.70	0	11	Q(12)	64 331.06
0	12	Q(3)	64 889.86	0	12	S(3)	64 998.96
0	12	Q(4)	64 781.77	0	12	Q(5)	64 654.02
0	12	S(5)	64 811.24	0	12	O(6)	64 376.07
0	12	Q(6)	64 511.40	0	12	O(7)	64 199.67
0	12	Q(7)	64 357.58	0	12	S(7)	64 562.72
0	12	O(8)	64 024.42	0	12	O(9)	63 849.55
0	12	Q(9)	64 055.69	0	12	S(9)	64 305.57
0	12	O(10)	63 696.70	0	12	Q(10)	63 924.40
0	13	Q(3)	63 905.42	0	13	Q(4)	63 841.87
0	13	O(5)	63 661.97	0	13	Q(5)	63 771.65
0	12	Q(0)	65 060.68	0	12	Q(1)	65 032.35
0	12	O(4)	64 696.16	0	13	Q(0)	64 011.54
0	13	S(0)	64 051.74	0	13	Q(1)	63 993.60
1	6	O(23)	66 308.66	1	7	O(21)	66 120.98
1	7	Q(21)	66 570.35	1	8	O(19)	65 887.53
1	8	Q(19)	66 299.74	1	9	Q(16)	66 343.24
1	9	Q(17)	65 990.07	1	10	Q(12)	66 566.23
1	10	Q(13)	66 236.87	1	10	Q(14)	65 928.48
1	10	Q(15)	65 655.57	1	11	Q(8)	66 460.64
1	11	Q(9)	66 214.56	1	11	Q(12)	65 504.24
1	12	Q(9)	65 238.30	1	12	O(10)	64 881.97
1	12	Q(10)	65 105.98	1	13	S(7)	65 027.54
1	12	Q(7)	65 545.67	1	13	Q(0)	65 207.25
1	13	Q(1)	65 188.76	1	13	S(1)	65 247.84
1	13	Q(2)	65 151.55	1	13	O(3)	65 038.08
1	13	Q(3)	65 099.52	1	13	O(5)	64 853.59
1	13	Q(5)	64 963.13	1	13	S(5)	65 116.96
1	13	Q(6)	64 892.62	1	13	O(7)	64 670.11
1	13	Q(7)	64 825.66	1	14	O(4)	64 477.19
2	12	Q(9)	66 370.16	2	12	S(9)	66 610.39
2	13	S(4)	66 299.74	2	13	O(7)	65 807.52
2	13	Q(7)	65 959.96	2	14	Q(1)	65 720.46
2	14	O(2)	65 675.34	2	14	Q(2)	65 711.49
2	14	S(1)	65 777.95	2	14	Q(3)	65 700.67

In an alternative scheme, following the methods of multi-channel quantum-defect theory (MQDT) an accuracy at the level of few cm^{-1} was achieved for reported levels in the $E^1\Sigma_g^+$ inner well of H_2 [9]. Comparison with the present accurate determination of energies for F-levels shows that for F0-levels up to $J = 13$ the MQDT-calculations yield values that are all higher by 1.4 cm^{-1}, and smoothly increasing to an excess of 1.6 cm^{-1} at $J = 19$. For the low-J levels of F1 the MQDT-values are consistently higher by 4.3 cm^{-1}. These comparisons with MQDT results for H_2 are displayed in Fig. 10.

For the present assignments and analysis ab initio calculations are performed for ro-vibrational level energies the $EF^1\Sigma_g^+$ double-well state. We employ the coupled-channel approach described in Ref. [33]

Table 12
HD linelist.

v_F	v_X	Line	Freq.	v_F	v_X	Line	Freq.
0	7	Q(26)	65 910.49	0	8	O(24)	65 278.27
0	8	Q(23)	66 131.28	0	8	Q(24)	65 677.54
0	9	Q(20)	66 237.79	0	9	Q(21)	65 808.52
0	9	Q(22)	65 405.57	0	9	Q(23)	65 040.85
0	10	O(18)	65 512.86	0	10	Q(17)	66 208.30
0	10	O(19)	65 126.52	0	10	Q(18)	65 820.40
0	10	Q(19)	65 449.31	0	10	Q(20)	65 101.79
0	10	Q(21)	64 791.43	0	10	S(20)	65 472.05
0	10	S(21)	65 177.87	0	11	O(14)	65 790.64
0	11	Q(13)	66 369.71	0	11	O(15)	65 440.48
0	11	Q(14)	66 032.76	0	11	O(16)	65 097.61
0	11	O(17)	64 770.99	0	11	S(14)	66 307.97
0	11	Q(16)	65 372.29	0	11	O(18)	64 466.84
0	11	Q(17)	65 063.71	0	11	S(17)	65 385.50
0	11	Q(19)	64 520.56	0	11	S(18)	65 113.32
0	12	O(9)	66 058.38	0	12	Q(9)	66 212.27
0	12	Q(10)	65 960.18	0	12	O(12)	65 224.01
0	12	Q(11)	65 698.30	0	12	O(13)	64 942.15
0	12	Q(12)	65 431.69	0	12	O(14)	64 664.34
0	12	Q(13)	65 165.40	0	12	O(15)	64 400.09
0	12	S(12)	65 673.24	0	12	Q(14)	64 905.45
0	12	O(16)	64 157.36	0	12	S(13)	65 423.51
0	12	Q(15)	64 658.65	0	12	Q(16)	64 433.57
0	12	S(15)	64 951.92	0	13	Q(0)	66 102.10
0	13	Q(2)	66 019.09	0	13	Q(3)	65 939.12
0	13	Q(4)	65 833.49	0	13	Q(5)	65 705.22
0	13	Q(6)	65 557.70	0	13	O(8)	65 074.39
0	13	Q(7)	65 391.40	0	13	O(9)	64 867.03
0	13	Q(8)	65 212.15	0	13	O(10)	64 655.98
0	13	S(7)	65 546.36	0	13	Q(9)	65 023.09
0	13	Q(10)	64 825.92	0	13	O(12)	64 229.23
0	13	Q(11)	64 629.52	0	13	O(13)	64 030.79
0	13	S(10)	65 034.18	0	13	Q(12)	64 437.44
0	13	S(11)	64 855.29	0	13	Q(13)	64 255.76
0	13	S(12)	64 678.28	0	13	Q(14)	64 094.35
0	13	S(13)	64 514.57	0	14	O(3)	64 740.57
0	14	Q(2)	64 848.77	0	14	Q(3)	64 785.54
0	14	Q(4)	64 704.94	0	14	Q(5)	64 607.02
0	14	Q(6)	64 496.31	0	14	S(5)	64 725.84
0	14	Q(7)	64 374.74	0	14	Q(8)	64 248.71
0	14	Q(9)	64 116.85	0	14	Q(10)	63 991.87
0	14	S(9)	64 307.14	0	14	Q(11)	63 876.61
0	14	S(11)	64 101.46	0	15	Q(1)	63 986.80
0	15	Q(2)	63 957.38	0	15	Q(3)	63 916.32
0	15	Q(4)	63 863.43	0	15	Q(5)	63 801.30
0	15	Q(6)	63 736.63	1	8	O(24)	66 276.52
1	10	O(20)	65 776.08	1	10	Q(19)	66 456.76
1	11	Q(16)	66 390.80	1	11	Q(17)	66 076.65
1	12	Q(13)	66 191.40	1	12	Q(14)	65 929.67
1	12	Q(17)	65 255.86	1	12	S(17)	65 572.00
1	13	Q(8)	66 248.12	1	13	Q(12)	65 465.48
1	13	Q(13)	65 282.80	1	13	Q(14)	65 121.73
1	13	S(13)	65 534.97	1	14	Q(7)	65 413.09
1	14	Q(8)	65 284.36	1	14	Q(9)	65 152.16
1	14	O(11)	64 721.76	1	14	Q(12)	64 812.33
1	15	Q(2)	64 999.29	1	15	Q(3)	64 958.24
1	15	O(5)	64 761.69	1	15	S(2)	65 059.50
1	15	Q(5)	64 842.24	1	15	Q(6)	64 774.71
1	15	Q(7)	64 707.07	1	15	Q(8)	64 643.85
1	15	Q(9)	64 591.99	1	16	Q(3)	64 413.41
2	12	Q(16)	66 430.36	2	13	Q(14)	66 102.40
2	14	O(7)	66 294.74	2	14	Q(7)	66 410.03
2	15	Q(8)	65 639.21	2	15	S(8)	65 804.57
2	16	Q(4)	65 396.35	3	16	Q(1)	66 400.68
3	17	Q(0)	66 177.53				

which includes the first five excited $^1\Sigma_g^+$ states. The term values of the EF($v < 6, J = 0 - 5$) states could be reproduced using the original ab initio data obtained by Wolniewicz and coworkers for the BO potential energy curves, adiabatic corrections and homogeneous electronic coupling functions [4]. For the term values presented in this work, the more accurate BO potential energy curves calculated by Silkowski and coworkers [53] were used, which lowered the energies by about 1 cm^{-1}. Heterogeneous couplings between the EF state and excited $^1\Pi_g^+$ were neglected, due to a lack of ab initio data for $\left\langle {}^1\Pi_g^+ | L^+ | \mathrm{EF} \right\rangle$. This seems justified in view of the 2sσ character of the EF state and taking into account that a pure precession model predicts only mixing between 3dσ − 3dπ. For the outer-well F levels with low vibrational excitation, no appreciable 3d character is expected and test calculations including the GK-I heterogeneous coupling result in energy shifts below 0.1 cm^{-1} even for $J = 23$ in H_2. Relativistic and QED corrections for E($v = 0$) were found to be of the order of 0.1 cm^{-1} [62] and were therefore neglected in the current work.

Results of these calculations are included in the various Tables with experimental data on F-levels for H_2 (Tables 3 and 4), for HD (Tables 5, 6, and 7) and D_2 (Tables 8, 9, and 10).

The calculations of the level energies of the $F^1\Sigma_g^+$ outer well states can be compared to the level energies assigned from experiment. For this purpose in Fig. 10 a comparison is made between the experimental and theoretical values as obtained for two data sets pertaining to H_2. The first panel shows for the high-resolution data in the rotational manifold for F0, a constant offset for the MQDT results, and a gradually increasing offset for the present nonadiabatic calculations as a function of J. The smoothness of the curves indicates that there are no outliers that should be interpreted as misassignments.

The second panel of Fig. 10 shows the data for the F1 manifold as obtained from the low-resolution spectra. An outlier is found for the nonadiabatic calculations of the F1($J = 6$) level, which is off by some 2 cm^{-1}, while all other deviations smoothly follow a decreasing trend from low J up to a deviation of −3.6 cm^{-1} at $J = 21$. A similar offset is found in the comparison with MQDT data. In view of this rather strong deviation the assignment of the F1($J = 6$) level in Table 4 is marked as tentative. Indeed, this level was observed in only one transition.

A similar deviation is found for the F1($J = 4$) level in HD, displayed in Fig. 10(c), where the calculated value is higher by 2.8 cm^{-1}, while all other deviations are below 1 cm^{-1}. This assignment for the F0($J = 24$) level in D_2, see Fig. 10(d), is also marked as tentative.

The J-dependent deviation between experimental and non-adiabatic term values, especially for H_2 and HD, indicates missing heterogeneous couplings with excited $^1\Pi_g^+$ states, which would lower the theoretical F0 and F1 term values. To improve the coupled-channel calculations, ab inito data for $\langle L^+ \rangle$ coupling elements is needed. In contrast, MQDT treats homogeneous and heterogeneous non-adiabatic effects naturally on the same footing and the constant offset in Fig. 10 might be reduced drastically by repeating the MQDT calculation with quantum defects extracted from the new ab initio BO potential energy curves.

Recently, the four-body calculations of the inner well E states [62] were extended to the rotational ground state of the outer F well [63], resulting in a term value of 99 365(1) cm^{-1} for F(0,0). As can be seen from the first entry in Table 3, this deviates by −1.2 cm^{-1} from the experimental value, compared to a 0.3 cm^{-1} discrepancy resulting from a comparison with the coupled-channel approach. While four-body calculations allow ultimately to reach higher accuracies, they remain computationally challenging for large R and high J.

7. Conclusion

In the present study vibrationally and rotationally excited states in the $X^1\Sigma_g^+$ electronic ground states of H_2, HD and D_2 fragment species were produced via two-photon ultraviolet photolysis of H_2S, HDS and D_2S, respectively. These states, with wave function density at large internuclear separation, were subjected to laser spectroscopic investigations of the $F^1\Sigma_g^+$ - $X^1\Sigma_g^+$ system in the hydrogen isotopologues. Combined with known accurate theoretical values for the X(v, J) levels [35,36,52], level energies of series of rotational states in the $F^1\Sigma_g^+$ outer well state were determined up to high angular momentum. In H_2 results were obtained via a high-resolution three-color laser scheme for

Table 13
D_2 linelist.

v_F	v_X	Line	Freq.	v_F	v_X	Line	Freq.
0	10	Q(29)	65 682.19	0	11	Q(24)	66 509.52
0	11	Q(26)	65 787.37	0	11	Q(27)	65 449.94
0	12	Q(20)	66 826.12	0	12	Q(21)	66 481.00
0	12	Q(23)	65 812.66	0	12	Q(24)	65 494.50
0	13	Q(17)	66 647.29	0	13	Q(18)	66 345.49
0	13	Q(19)	66 044.44	0	13	Q(20)	65 748.88
0	13	Q(21)	65 460.65	0	13	Q(22)	65 184.22
0	14	Q(17)	65 588.82	0	14	Q(18)	65 336.29
0	14	Q(19)	65 091.05	0	14	S(17)	65 807.90
0	14	S(18)	65 567.20	0	15	Q(6)	66 766.96
0	15	Q(7)	66 627.87	0	15	Q(8)	66 476.58
0	15	Q(9)	66 308.67	0	15	Q(11)	65 938.80
0	15	Q(12)	65 742.01	0	15	Q(13)	65 537.97
0	15	O(16)	64 728.82	0	15	Q(14)	65 327.24
0	15	Q(15)	65 122.32	0	15	Q(16)	64 914.63
0	15	S(14)	65 515.41	0	15	S(17)	64 933.43
0	16	Q(13)	64 655.44	0	16	Q(4)	65 859.20
0	16	Q(5)	65 771.20	0	16	O(8)	65 331.49
0	16	Q(6)	65 668.79	0	16	Q(7)	65 551.35
0	16	Q(8)	65 421.55	0	16	Q(9)	65 281.49
0	16	S(7)	65 655.20	0	16	O(12)	64 678.32
0	16	Q(10)	65 131.89	0	16	Q(11)	64 977.58
0	16	Q(12)	64 816.94	0	16	S(10)	65 272.84
0	17	Q(4)	64 897.35	0	17	Q(5)	64 825.02
0	17	Q(6)	64 740.84	0	17	S(7)	64 749.95
0	17	O(12)	63 947.24	0	17	Q(11)	64 203.54
0	17	Q(12)	64 088.77	0	17	Q(2)	65 000.13
0	18	S(4)	64 185.23	0	18	Q(1)	64 219.44
0	18	Q(2)	64 195.02	0	18	S(2)	64 238.44
0	20	S(3)	63 267.84	1	10	Q(29)	66 494.72
1	11	Q(26)	66 608.29	1	12	Q(23)	66 641.46
1	12	Q(24)	66 322.34	1	13	Q(20)	66 584.83
1	13	Q(21)	66 294.44	1	13	Q(22)	66 015.62
1	14	Q(16)	66 688.32	1	14	Q(17)	66 431.15
1	14	Q(19)	65 928.48	1	14	Q(20)	65 691.85
1	15	Q(11)	66 789.99	1	15	Q(12)	66 591.64
1	15	Q(13)	66 385.98	1	15	Q(15)	65 967.18
1	15	Q(19)	65 179.15	1	16	Q(11)	65 828.38
1	16	Q(14)	65 339.16	1	16	Q(17)	64 895.09
1	16	Q(4)	66 717.04	1	16	Q(6)	66 523.54
1	16	Q(7)	66 406.87	1	16	S(6)	66 614.36
1	17	O(12)	64 800.23	1	17	Q(10)	65 171.10
1	17	Q(11)	65 052.64	1	17	Q(12)	64 937.89
1	17	Q(15)	64 624.84	1	18	S(8)	64 831.26
1	18	S(9)	64 769.49	1	18	Q(2)	65 052.23
1	18	Q(3)	65 017.30	1	18	Q(4)	64 973.60
1	18	Q(5)	64 920.35	1	18	Q(6)	64 858.44
1	18	Q(7)	64 790.97	1	18	Q(8)	64 717.59
1	19	O(8)	64 170.87	1	20	Q(0)	64 082.43
2	17	Q(5)	66 507.91	2	18	Q(4)	65 802.74
2	17	Q(11)	65 879.61	2	17	Q(12)	65 760.99
2	17	Q(15)	65 446.28	2	18	Q(2)	65 883.04
2	18	Q(3)	65 845.22	2	19	Q(4)	65 229.39
2	20	Q(0)	64 910.20	3	19	Q(8)	65 889.37
4	19	S(5)	66 846.32				

$v_F = 0, 1$ at typical uncertainties of 5×10^{-3} cm^{-1}. In addition, from a lower resolution two-color laser scheme additional $v_F = 0, 1$ levels as well as $v_F = 2$ levels were determined at an accuracy of 0.5 cm^{-1}. For HD and D_2 energies of many F-levels $v_F = 0-4$ were determined for the first time. Also, for the first time a quasi-bound resonance, for ($v = 17$, $J = 15$), was observed on the electronic ground state potential of D_2.

Full non-adiabatic term values for the $F^1\Sigma_g^+$ outer well levels were calculated for all three isotopologues, based on a coupled-channel approach including $^1\Sigma_g^+$ states. Good agreement, at the level of the experimental accuracy of 0.5 cm^{-1}, is obtained from these calculations.

Declaration of competing interest

The authors declare that they have no known competing financial interests or personal relationships that could have appeared to influence the work reported in this paper.

Data availability

Data will be made available on request.

Acknowledgments

This work was financially supported by the European Research Council through an ERC Advanced grant (No. 670168). MB acknowledges Netherlands Organisation for Scientific Research for a VENI grant (VI.Veni.202.140).

Appendix

In this Appendix line lists will be provided on the measured frequencies of the $F^1\Sigma_g^+$ - $X^1\Sigma_g^+$ two-photon transitions in all three isotopologues, Table 11 for H_2, Table 12 for HD, and Table 13 for D_2. The listed data are acquired via the low-resolution two-color scheme for which an uncertainty of 0.5 cm^{-1} is determined. All values in cm^{-1}.

References

[1] G.H. Dieke, The $2s^1\Sigma \rightarrow 2p^1\Sigma$ bands of the hydrogen molecule, Phys. Rev. 50 (1936) 797.
[2] G.H. Dieke, Bands from doubly excited levels of the hydrogen molecule, Phys. Rev. 76 (1949) 50.
[3] E. Davidson, First excited $^1\Sigma_g^+$ state of the hydrogen molecules, J. Chem. Phys. 35 (1961) 1189.
[4] S. Yu, K. Dressler, Calculation of rovibronic structures in the lowest nine excited $^1\Sigma_g^+ + {}^1\Pi_g + {}^1\Delta_g$ states of H_2, D_2, and T_2, J. Chem. Phys. 101 (1994) 7692.
[5] D. Shiner, J.M. Gilligan, B.M. Cook, W. Lichten, H_2, D_2, and HD ionization potentials by accurate calibration of several iodine lines, Phys. Rev. A 47 (1993) 4042.
[6] Y.P. Zhang, C.H. Cheng, J.T. Kim, J. Stanojevic, E.E. Eyler, Dissociation energies of molecular hydrogen and the hydrogen molecular ion, Phys. Rev. Lett. 92 (2004) 203003.
[7] S. Hannemann, E.J. Salumbides, S. Witte, R.T. Zinkstok, E.J. van Duijn, K.S.E. Eikema, W. Ubachs, Frequency metrology on the $EF^1\Sigma_g^+ - X^1\Sigma_g^+$ (0, 0) transition in H_2, HD, and D_2, Phys. Rev. A 74 (2006) 062514.
[8] E.J. Salumbides, G.D. Dickenson, T.I. Ivanov, W. Ubachs, QED effects in molecules: Test on rotational quantum states of H_2, Phys. Rev. Lett. 107 (2011) 043005.
[9] G.D. Dickenson, E.J. Salumbides, M. Niu, C. Jungen, S.C. Ross, W. Ubachs, Precision spectroscopy of high rotational states in H_2 investigated by Doppler-free two-photon laser spectroscopy in the $EF^1\Sigma_g^+$-$X^1\Sigma_g^+$ system, Phys. Rev. A 86 (2012) 032502.
[10] R.K. Altmann, L.S. Dreissen, E.J. Salumbides, W. Ubachs, K.S.E. Eikema, Deep-ultraviolet frequency metrology of H_2 for tests of molecular quantum theory, Phys. Rev. Lett. 120 (2018) 043204.
[11] R.S. Mulliken, Rare-gas and hydrogen molecule electronic states, noncrossing rule, and recombination of electrons with rare-gas and hydrogen ions, Phys. Rev. 136 (1964) A962.
[12] K. Dressler, L. Wolniewicz, The $I^1\Pi_g$ state of hydrogen: adiabatic corrections, energy levels, L-uncoupling, and electronic transition moments, Can. J. Phys. 62 (1984) 1706.
[13] E. Reinhold, A. de Lange, W. Hogervorst, W. Ubachs, Observation of the $I'^1\Pi_g$ outer well state in H_2 and D_2, J. Chem. Phys. 109 (1998) 9772.
[14] A. de Lange, E. Reinhold, W. Hogervorst, W. Ubachs, Gerade/ungerade symmetry-breaking in HD at the n=2 dissociation limit, Can. J. Phys. 78 (2000) 567.
[15] D. Sprecher, M. Beyer, F. Merkt, Precision measurement of the ionisation energy of the $3d\sigma$ GK state of H_2, Mol. Phys. 111 (2013) 2100.
[16] N. Hölsch, M. Beyer, F. Merkt, Nonadiabatic effects on the positions and lifetimes of the low-lying rovibrational levels of the GK $^1\Sigma_g^+$ and H $^1\Sigma_g^+$ states of H_2, Phys. Chem. Chem. Phys. 20 (2018) 26837.
[17] E. Reinhold, W. Hogervorst, W. Ubachs, Observation of a highly excited long-lived valence state in H_2, Phys. Rev. Lett. 78 (1997) 2543.
[18] A. de Lange, W. Hogervorst, W. Ubachs, Double-well states of ungerade symmetry in H_2: First observation and comparison with ab initio calculations, Phys. Rev. Lett. 86 (2001) 2988.
[19] E. Reinhold, W. Hogervorst, W. Ubachs, L. Wolniewicz, Experimental and theoretical investigation of the $H\overline{H}^1\Sigma_g^+$ state in H_2, D_2, and HD, and the $B\overline{B}^1\Sigma_u^+$ state in HD, Phys. Rev. A 60 (1999) 1258.
[20] T. Detmer, P. Schmelcher, L.S. Cederbaum, Ab initio calculations with a non-spherical Gaussian basis set: Excited states of the hydrogen molecule, J. Chem. Phys. 109 (1998) 9694.

[21] J.C.J. Koelemeij, A. de Lange, W. Ubachs, Search for outer-well states above the ionization potential in H_2, Chem. Phys. 287 (2003) 349.

[22] D. Bailly, E. Salumbides, M. Vervloet, W. Ubachs, Accurate level energies in the $EF^1\Sigma_g^+$, $GK^1\Sigma_g^+$, $H^1\Sigma_g^+$, $B^1\Sigma_u^+$, $C^1\Pi_u$, $B'^1\Sigma_u^+$, $D^1\Pi_u$, $I^1\Pi_g$, $J^1\Delta_g$ states of H_2, Mol. Phys. 108 (2010) 827.

[23] E.J. Salumbides, D. Bailly, M. Vervloet, W. Ubachs, $B^1\Sigma_u^+$ and $EF^1\Sigma_g^+$ level energies of D_2, J. Mol. Spectrosc. 305 (2014) 34.

[24] E.E. Marinero, R. Vasudev, R.N. Zare, The E,F $^1\Sigma_g^+$ double-minimum state of hydrogen: Two-photon excitation of inner and outer wells, J. Chem. Phys. 78 (1983) 692.

[25] J. Steadman, T. Baer, The production and characterization by resonance enhanced multiphoton ionization of H_2 ($v = 10 - 14$) from photodissociation of H_2S, J. Chem. Phys. 91 (1989) 6113.

[26] M.L. Niu, E.J. Salumbides, W. Ubachs, Communication: Test of quantum chemistry in vibrationally hot hydrogen molecules, J. Chem. Phys. 143 (2015) 081102.

[27] T.M. Trivikram, M.L. Niu, P. Wcisło, W. Ubachs, E.J. Salumbides, Precision measurements and test of molecular theory in highly excited vibrational states of H_2 ($v = 11$), Appl. Phys. B 122 (2016) 294.

[28] T.M. Trivikram, E.J. Salumbides, C. Jungen, W. Ubachs, Excitation of H_2 at large internuclear separation: outer well states and continuum resonances, Mol. Phys. 117 (2019) 2961.

[29] K.-F. Lai, M. Beyer, E.J. Salumbides, W. Ubachs, Photolysis production and spectroscopic investigation of the highest vibrational states in H_2 ($X^1\Sigma_g^+$ $v = 13, 14$), J. Phys. Chem. A 125 (2021) 1221.

[30] K.-F. Lai, E.J. Salumbides, W. Ubachs, M. Beyer, Shape resonances in H_2 as photolysis reaction intermediates, Phys. Rev. Lett. 127 (2021) 183001.

[31] K.-F. Lai, E.J. Salumbides, M. Beyer, W. Ubachs, Precision measurement of quasi-bound resonances in H_2 and the H+H scattering length, Mol. Phys. 120 (2022).

[32] M.S. Quinn, K. Nauta, S.H. Kable, Disentangling the H_2 $EF(^1\Sigma_g^+)$ ($v' = 0 - 18$) - X ($^1\Sigma_g^+$) ($v = 3 - 9$) (2+1) REMPI spectrum via 2D velocity-mapped imaging, Mol. Phys. 119 (2020) e1836412.

[33] P. Quadrelli, K. Dressler, L. Wolniewicz, Nonadiabatic coupling between the EF + GK + $H^1\Sigma_g^+$, $I^1\Pi_g$, and $J^1\Delta_g$ states of the hydrogen molecule. Calculation of rovibronic structures in H_2, HD, and D_2, J. Chem. Phys. 92 (1990) 7461.

[34] G.H. Dieke, M.N. Lewis, Bands of HD and D_2 ending on the $2p^1\Sigma$ state, Phys. Rev. 52 (1937) 100.

[35] P. Czachorowski, M. Puchalski, J. Komasa, K. Pachucki, Nonadiabatic relativistic correction in H_2, D_2, and HD, Phys. Rev. A 98 (2018) 052506.

[36] K. Pachucki, J. Komasa, Nonrelativistic energy of D_2, Phys. Chem. Chem. Phys. 21 (2019) 10272.

[37] M.N.R. Ashfold, W.S. Hartree, A.V. Salvato, B. Tutcher, A. Walker, A reinvestigation of the Rydberg states of H_2S and D_2S by two-photon resonant multiphoton ionisation spectroscopy, J. Chem. Soc. Faraday Trans. 86 (1990) 2027.

[38] J. Zhou, Y. Zhao, C.S. Hansen, J. Yang, Y. Chang, Y. Yu, G. Cheng, Z. Chen, Z. He, S. Yu, H. Ding, W. Zhang, G. Wu, D. Dai, C.M. Western, M.N. Ashfold, K. Yuan, X. Yang, Ultraviolet photolysis of H_2S and its implications for SH radical production in the interstellar medium, Nat. Commun. 11 (2020) 1547.

[39] Y. Zhao, Z. Luo, Y. Chang, Y. Wu, S. Zhang, Z. Li, H. Ding, G. Wu, J.S. Campbell, C.S. Hansen, S.W. Crane, C.M. Western, M.N.R. Ashfold, K. Yuan, X. Yang, Rotational and nuclear-spin level dependent photodissociation dynamics of H_2S, Nat. Commun. 12 (2021) 4459.

[40] G. Tarczay, A.G. Császár, O.L. Polyansky, J. Tennyson, Ab initio rovibrational spectroscopy of hydrogen sulfide, J. Chem. Phys. 115 (2001) 1229.

[41] I. Kozin, P. Jensen, Fourfold clusters of rovibrational energy levels for H_2S studied with a potential energy surface derived from experiment, J. Mol. Spectrosc. 163 (1994) 483.

[42] S. Miller, J. Tennyson, P. Rosmus, J. Senekowitsch, I.M. Mills, Calculated rotational and rovibrational spectra of D_2S and HDS, J. Mol. Spectrosc. 143 (1990) 61.

[43] O. Ulenikov, G. Onopenko, I. Olekhnovitch, S. Alanko, V.-M. Horneman, M. Koivusaari, R. Anttila, High-resolution Fourier transform spectra of HDS in the regions of the bands ν_1 and $2\nu_1/\nu_2 + \nu_3$, J. Mol. Spectrosc. 189 (1998) 74.

[44] A.-W. Liu, O. Ulenikov, G. Onopenko, O. Gromova, E. Bekhtereva, L. Wan, L.-Y. Hao, S.-M. Hu, J.-M. Flaud, Global fit of the high-resolution infrared spectrum of D_2S, J. Mol. Spectrosc. 238 (2006) 11.

[45] C. Kreis, U. Hollenstein, F. Merkt, Threshold-ion-pair-production spectroscopy of H_2S and D_2S, Mol. Phys. 120 (2022) e2071349.

[46] X. Zheng, J. Wu, Y. Song, J. Zhang, Ultraviolet photodissociation of the SD radical in vibrationally ground and excited states, Phys. Chem. Chem. Phys. 11 (2009) 4761.

[47] O.V. Boyarkin, M.A. Koshelev, O. Aseev, P. Maksyutenko, T.R. Rizzo, N.F. Zobov, L. Lodi, J. Tennyson, O.L. Polyansky, Accurate bond dissociation energy of water determined by triple-resonance vibrational spectroscopy and ab initio calculations, Chem. Phys. Lett. 14 (2013) 568–569.

[48] L.R. Brown, J.A. Crisp, D. Crisp, O.V. Naumenko, M.A. Smirnov, L. Sinitsa, A. Perrin, The absorption spectrum of H_2S between 2150 and 4260 cm^{-1}: Analysis of the positions and intensities in the first ($2\nu_2$, ν_1, and ν_3) and second ($3\nu_2$, $\nu_1 + \nu_2$, and $\nu_2 + \nu_3$) triad regions, J. Mol. Spectrosc. 188 (1998) 148.

[49] M.L. Niu, E.J. Salumbides, G.D. Dickenson, K.S.E. Eikema, W. Ubachs, Precision spectroscopy of the $X^1\Sigma_g^+, v = 0 \rightarrow 1\,(J = 0-2)$ rovibrational splittings in H_2, HD and D_2, J. Mol. Spectrosc. 300 (2014) 44.

[50] S. Gerstenkorn, P. Luc, Atlas Du Spectre D'Absorption de la Molecule D'Iode 15600 – 17600 Cm^{-1}, Laboratoire Aimé Cotton, CNRS II, 91405 Orsay, France, 1977.

[51] M. Wolfsberg, A.A. Massa, J.W. Pyper, Effect of vibrational anharmonicity on the isotopic self-exchange equilibria $H_2X + D_2X=2$ HDX, J. Chem. Phys. 53 (1970) 3138.

[52] H2SPECTRE Ver 7.4 Fortran Source Code, University of Warsaw, Poland, 2022.

[53] M. Siłkowski, M. Zientkiewicz, K. Pachucki, Accurate Born–Oppenheimer potentials for excited Σ^+ states of the hydrogen molecule, Adv. Quant. Chem. 83 (2021) 255.

[54] T. Srinivasan, H. Egger, T. Luk, H. Pummer, C. Rhodes, The influence of the optical stark shift on the two-photon excitation of the molecular hydrogen $EF^1\Sigma_g^+$ state, IEEE J. Quant. Electr. 19 (1983) 1874.

[55] M.J.J. Vrakking, A.S. Bracker, T. Suzuki, Y.T. Lee, Ultrasensitive detection of hydrogen molecules by (2+1) resonance-enhanced multiphoton ionization, Rev. Sci. Instrum. 64 (1993) 3.

[56] A. Yiannopoulou, N. Melikechi, S. Gangopadhyay, J.C. Meiners, C.H. Cheng, E.E. Eyler, Determinations of $EF^1\Sigma_g^+$ - $X^1\Sigma_g^+$ transition frequencies in H_2, D_2, and HD, Phys. Rev. A 73 (2006) 022506.

[57] G.D. Dickenson, M.L. Niu, E.J. Salumbides, J. Komasa, K.S.E. Eikema, K. Pachucki, W. Ubachs, Fundamental vibration of molecular hydrogen, Phys. Rev. Lett. 110 (2013) 193601.

[58] M. Selg, Observable quasi-bound states of the H_2 molecule, J. Chem. Phys. 136 (2012) 114113.

[59] C.R. Scheper, C.A. de Lange, A. de Lange, E. Reinhold, W. Ubachs, Dissociation of H_2 in the energy region at the H(n=1)+H(n=3) dissociation threshold after (1+1') resonance-enhanced two-photon ionization via the $B^1\Sigma_u^+$ state, Chem. Phys. Lett. 312 (1999) 131.

[60] N. Hölsch, M. Beyer, E.J. Salumbides, K.S.E. Eikema, W. Ubachs, C. Jungen, F. Merkt, Benchmarking theory with an improved measurement of the ionization and dissociation energies of H_2, Phys. Rev. Lett. 122 (2019) 103002.

[61] M. Puchalski, J. Komasa, P. Czachorowski, K. Pachucki, Nonadiabatic QED correction to the dissociation energy of the hydrogen molecule, Phys. Rev. Lett. 122 (2019) 103003.

[62] D. Ferenc, E. Mátyus, Computation of rovibronic resonances of molecular hydrogen: $EF^1\Sigma_g^+$ inner-well rotational states, Phys. Rev. A 100 (2019) 020501.

[63] E. Saly, D. Ferenc, E. Mátyus, Pre-Born–Oppenheimer energies, leading-order relativistic and QED corrections for electronically excited states of molecular hydrogen, Mol. Phys. (2023) e2163714.